CONTROL SYSTEM DESIGN FOR DISTURBANCE REJECTION IN ACTIVE VIBRATION CONTROL SYSTEMS

A Project Presented to

The Faculty of the Department of

Mechanical Engineering

San Jose State University

In Partial Fulfillment

of the Requirements for the Degree

Master of Science

in

Mechanical Engineering

by

Alireza Mounesisohi

May 2017

SAN JOSE STATE UNIVERSITY

The Undersigned Committee Approves

Control System Design for Disturbance Rejection in Active Vibration Control Systems

of

Alireza Mounesisohi

APPROVED FOR THE DEPARTMENT OF MECHANICAL ENGINEERING

Dr. Saeid Bashash, Committee Chair	Date
Dr. Fred Barez, Committee Member	Date
Dr. Ali Rahimi, Committee Member	Date

ABSTRACT

Control Design for Disturbance Rejection in Active Vibration Control Systems

By Alireza Mounesisohi

The objective of this project is to control the vertical vibrations of a clamped-clamped beam subjected to external disturbances through a single-point position feedback using the data-driven control method. To achieve this goal, an experimental setup was designed and developed, comprising a flexible aluminum beam with two piezoelectric actuators and a laser sensor. The beam was experimentally characterized in the frequency domain, and a set of Frequency Response Data (FRD) models were created. More specifically, the beam was characterized via excitation at a known frequency using a piezoelectric actuator, while measuring the beam deflection with a laser sensor to determine amplitude and phase of the responses. Then, the plant response was computed in the frequency spectrum ranging from 0 to 500 Hz. A controller was then designed, and its parameters were optimized using the Nelder-Mead simplex search algorithm in MATLAB to achieve desirable closed-loop system objectives such as stability margins and sensitivity and open-loop transfer function shapes. The optimized controller was implemented in the dSPACE controller board to control the beam position while attenuating the effect of disturbances. Finally, the effectiveness of the technique was examined and validated through a set of experiments by random external disturbances and reference trajectory tracking.

ACKNOWLEDGEMENTS

I would like to acknowledge my committee chair, Dr. Saeid Bashash, for his dedication and support during the completion of the project. Dr. Bashash provided me an insight and guidance that greatly assisted my research path. His consideration inspired me to establish my skills in mechanical engineering and control system design and pursue higher levels of education. I appreciate my committee member, Dr. Fred Barez, for his supports and recommendations from the beginning of my study at San Jose State University. I would also like to thank Dr. Ali Rahimi for his productive class, Vibration of Mechanical Systems, and his additional supports during the project.

I would also like to show my gratitude to my family and friends for their continuous support in many aspects, especially my mother, my father, and my sisters.

TABLE OF CONTENTS

NOMENCLATURE

FRD	-	Frequency Response Data
PID	-	Proportional-Integral-Derivative
SISO	-	Single-Input-Single-Output
MIMO	-	Multi-Input-Multi-Output
AFM	-	Atomic Force Microscopy
VCM	-	Voice-Coil-Motor
HDD	-	Hard Disk Drive
LTI	-	Linear-Time-Invariant
CAD	-	Computer-Aided-Design
FEA	-	Finite Element Analysis
IFT	-	called Iterative Feedback Tuning
ICbT	-	Iterative Correlation based Tuning
DAC	-	Digital to Analog Converter
ADC	-	Analog to Digital Converter
FFT	-	Fast-Fourier-Transform
SNR	-	Signal to Noise Ratio
I/O	-	Input-Output
G(s)	-	transfer function in the s-domain
j or i	-	the imaginary unit
r(t)	-	reference signal
e(t)	-	error signal

LIST OF TABLES

LIST OF FIGURES

1.0 INTRODUCTION

Control systems engineering is an interdisciplinary field with numerous applications in mechanical, electrical, chemical, and computer engineering disciplines. Automatic control theory is applied to systems to obtain desired behavior such as reference tracking [1]. Control system is an organization of different components connected to each other to regulate, command, or govern the system to achieve desired behaviors. Input and output data are two key parameters that can characterize system dynamics [2]. Sensors are used to measure the experimental data from experiments and send the obtained data to a digital processor. A digital processor can be a micro-controller, a mini-controller, a micro-computer, or even a super computer. A controller has the capability to receive signals, process control laws, and send processed signals. The signal measured by the sensor is referred to as feedback signal and is transmitted to the processor. Based on the control system design, the controller corrects and adjusts the feedback signal to drive the actuator. This signal can be analog or digital depending on the application.

One early development of control system example is known to be the Ktesibios's water clock in Alexandria in Egypt over two thousand years ago [3]. The clock could keep time based on water level effect in a vessel. In 1868, James Clerk Maxwell demonstrated the flyball governor's equations of motion and described it as a control theory. By developing mathematical models for differential equations, the area of control theory has made significant advancements. By the advent of classical control theory, single-input-single-output (SISO) was studied. With the conventional technique, equations can be transformed from time domain to frequency domain using Fourier transform or Laplace transform. Proportional-integral-derivative (PID) controllers were the most functional controller in the classical theory. In addition to classical control theory, modern control theory is introduced to handle multi-input-multi-output (MIMO) systems.

Modern control theory has overcome the limitations of frequency response analysis in classical control methods [4]. The equations in modern control theory are set in a form of first order differential equations called state variables, and the controller is designed in a structured vector form, which allows systematical computing using advanced tools.

Applications of the control systems can be found in different industries such as robotics, marine, train systems, air-conditioning systems, speed regulators, position control of a beam, quadcopters, and test chamber temperature regulators.

1.1 Vibration Control

Noise and vibration have detrimental effects when considered as disturbances in control system design, and yet noise reduction is an essential engineering challenge to be solved. To reduce disturbances, three control methods have been proposed: passive, semi-active, and active. In any of above-mentioned methods, the experimental object which is exposed to vibrations needs to be characterized and modeled in its operating system based on a model, a controller needs to be designed and implemented, and results need to be evaluated.

In structural analysis, the method of active vibration control is used to mitigate seismic impacts in towers and buildings. With passive methods, the system doesn't acquire any feedback. An example of implementation of this technique is using a tuned mass-damper system in the middle of the building which the mass can freely swing from side to side [5]. Active control can also be used for such application. With this method, real-time sensors need to be installed on the building floor. When they are stimulated by for example earthquake, a signal will be conveyed towards the controller. The controller will process the signal and properly actives the actuators to stabilize the building.

Several vibration control approaches are used to prevent buildings from being damaged in an earthquake. The first method is to use seismic dampers in the superstructure of the building. The second method is dissipating the energy by breaking a high amplitude wave into a range of lower amplitudes waves. The third way is to use elevator capacity.

Noise reduction in dynamic applications is as attractive as well as structural one. In hard-disk-drive (HDD) data tracking applications [6]. Active vibration control is used to seek the desired data track and follows the tracking the presence of different disturbances sources such as air flutter and disk vibrations. The vibration control technique is also used to minimize noises and annoying vibrations of the arm's head. By suppressing the

vibration, data can be written or read in narrower tracks. Thus, more data can be stored in the same amount of the materials at a lower cost. Many other vibration control applications exist. For example aircraft, interior and fuselage noise reduction [7]; atomic force microscopy (AFM) imaging [8]; and active vehicle suspension system [9].

1.2 Active Vibration Control of Beam

Recently, many academic research efforts have been conducted on control system design of a beam structure. The beam structure has many advantages. The theoretical model of a simple beam can be found in the literature. The behavior of the beam is assumed to be a Linear-Time-Invariant (LTI) system. For a testbed development, a beam apparatus can be obtained from a metal supply. The beam can be mathematically modeled such as a cascade of second order differential equations which the amplitude of higher orders decays in higher frequencies.

Active vibration control of flexible beams has been widely used in the literature [10-12]. Khot et al. in [10] studied the vibration control of a cantilever beam, where the finite element model (FE model) of the system was designed using ANSYS. Then a PID controller was used to for the control system design. Zhang et al. in [11] presented vibration suppression for a smart cantilever beam. The cantilever beam was equipped with the piezoelectric actuators. Extended state observer was acquired during the state feedback control. The Hamilton principle was used to model the cantilever beam.

Another research work is conducted to investigate the active vibration of a flexible beam using system identification methods [12]. The dynamic model of the beam was identified using autoregression technique by recursive least squares. The physical model is tested using input and outputs. Then a PID controller was used and optimized via the evolutionary algorithms including differential evolution and genetic algorithm. The performance of the optimized PID controller was compared with the Ziegler and Nichols method. The results manifested the optimized PID controller functions better.

The vibration control has been examined with different sensor technologies. In [13] vibration control of smart cantilever beam was used with a strain gauge feedback. In this work, computer simulation and experimental results were compared. The Harmonic and

Modal analysis feature of ANSYS software was utilized for the computational analyses. Through the experiment, the dynamic model was obtained via system identification. The results verified the effectiveness of the controller in reducing the vibrations. Other references have used adaptive, robust, and nonlinear control methods for vibration suppression [14-17].

1.3 Data-Driven Control Design Method

Characterizing the system can be done with the mathematical modeling of the system. However, in some applications, obtaining an accurate model is challenged by the imperfect fabrication or the real-life uncertainties. Other methods are proposed in literature such as using finite element (FE) models or characterizing the system using a set of input and output (I/O) data. The latter approach is referred to as the data-driven design method. The advantages of the data-driven-method are:

- No need for model development (which could take up to 75% of the total design time [18])
- No need for analytical and finite element models
- For a given system, data-driven model is almost exact
- Scalable for large number of plants (useful consumer products, e.g., HDDs, smartphone cameras, etc.)
- Ability Accommodating numerous design objectives (stability, performance, robustness)

The disadvantages of the data driven-method are:

- Lack of insight into the physics of the system
- Non-conventional design (Frequency domain design vs. standard pole placement, LQR, etc.)
- Requirement for great level of expertise in the frequency domain design

- May require a significant amount of computations for controller optimization

Recently, the advancement of data-acquisition technology has made it feasible and straightforward to collect a large number of input and output measurements from experimental plants [20]. Consequently, data-driven control method has become more popular among control designers. Additionally, due to the limitations of physics-based modeling in sophisticated real-world systems, data-driven controllers could outperform the model-based designs with less overall design time. This method replaces the complicated physics-based ODE, state-space, or transfer function model with measured frequency-domain data, based on which a controller is developed and optimized in the frequency domain. Then the controller will be optimized for multiple closed-loop system objectives such as gain margin, phase margin, bandwidth, vibration amplitude, and robustness.

Gevers [18] discussed that the model development for control design is an expensive process, and estimated that 75% of the total cost of sophisticated control design is allocated only to modeling. In the data-driven method, the physical modeling of the system is not needed since the controller parameters can be directly optimized using experimentally obtained data [19]

After collecting data, the controller must be designed. There are many techniques to design and optimize the controller. S. Formentin proposed a method which is asymptotically exact, in that it guarantees that the desired closed-loop dynamics is matched when the number of data-points approach infinity [21]. Hjalmarsson proposed two practical iterative methods: Iterative Feedback Tuning (IFT) and Iterative Correlation based Tuning (ICbT) [22]. In IFT, an unbiased estimate of the gradient from input/output (I/O) data is collected from the actual closed-loop system. The second technique, ICbT, is developed for single-input-single-output (SISO) systems and extended for multi-input-multi-output MIMO systems later. Formentin et al. discussed multivariable controller based on the well-known Virtual Reference Feedback Tuning (VRFT). The method is developed based on a single set of input-output data collected on MIMO LTI square plant. However, important issues as under modeling and noise characteristics were not discussed [23].

Karimi *et al.* [24] presented a new robust control design for linear time-invariant single-input-single-output systems. The paper quantifies the effectiveness of the results

through an electrotechnical system. In the Data-Driven method, the controller is designed based on the collected data instead of using a parametric model of the plant. The paper also provided a method which proved sufficient and necessary conditions for the existence of robust controller that guarantees boundedness of the infinite norm on the closed loop system

The literature encompasses several model-based and data-driven control methods for vibration control such as H_2 and H_∞ [24, 25] , state-space [26], Lyapunov-based [27], and consensus control [28, 29]. The study in [6], the work aims at frequency domain data-driven control design to cancel the vibrations of a flexible beam like the one proposed for hard disk drives.

1.3 Project Objective

The goal of the project is to design control system for a smart, flexible structure to minimize disturbances and vibrations in the vertical direction. By acquiring a well-perform controller, the system can reject disturbances or follow a trajectory. A testbed is developed comprising an aluminum beam, laser sensor, and piezoelectric actuators. The controller is optimized based on the control system's targets such as stability margins, performance, and the overall shape of open-loop and error transfer function Bode plot.

2.0 SETUP CONFIGURATION

The control system configuration consists of a controller, a beam, and a disturbance source in a feedback loop system. Figure 1 presents the configuration of the closed-loop control system. The signals r(t), e(t), d(t), and y(t) are respectively, the reference signal, the error signal, the disturbance signal, and the output signal. The controller transfer function is $G_c(s)$, and the plant's transfer function is $G_p(s)$, both in the Laplace domain.

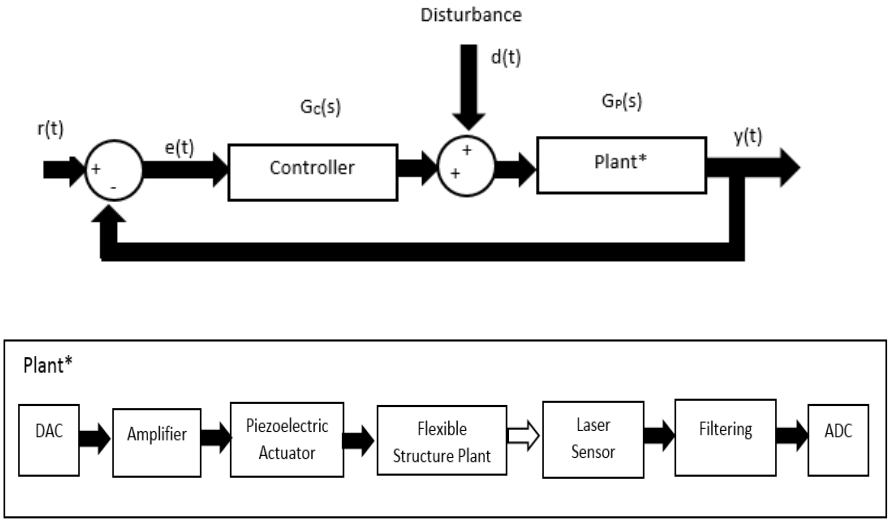

Figure 1 - Blok diagram of the smart beam control system design.

The block diagram representation unity feedback is used rather than the sensor feedback. Then the plant includes digital to analog converter (DAC), amplifier, piezoelectric actuators, the flexible beam structure, the sensor, sensor filtering, and analog to digital converter (ADC). Based on this configuration the output y(t) is the signal of the laser sensor which passes through the filtering and ADC. The laser's displacement data, approximately, is similar to the actual beam displacement.

2.1 Mechanical Structure

In the project, an experimental testbed is developed to validate the effectiveness of the controller. The test setup consists of a digital controller, flexible structure, a sensor, and actuators to comply with the configuration of the study. figure 2 shows the assembled components of the experimental setup.

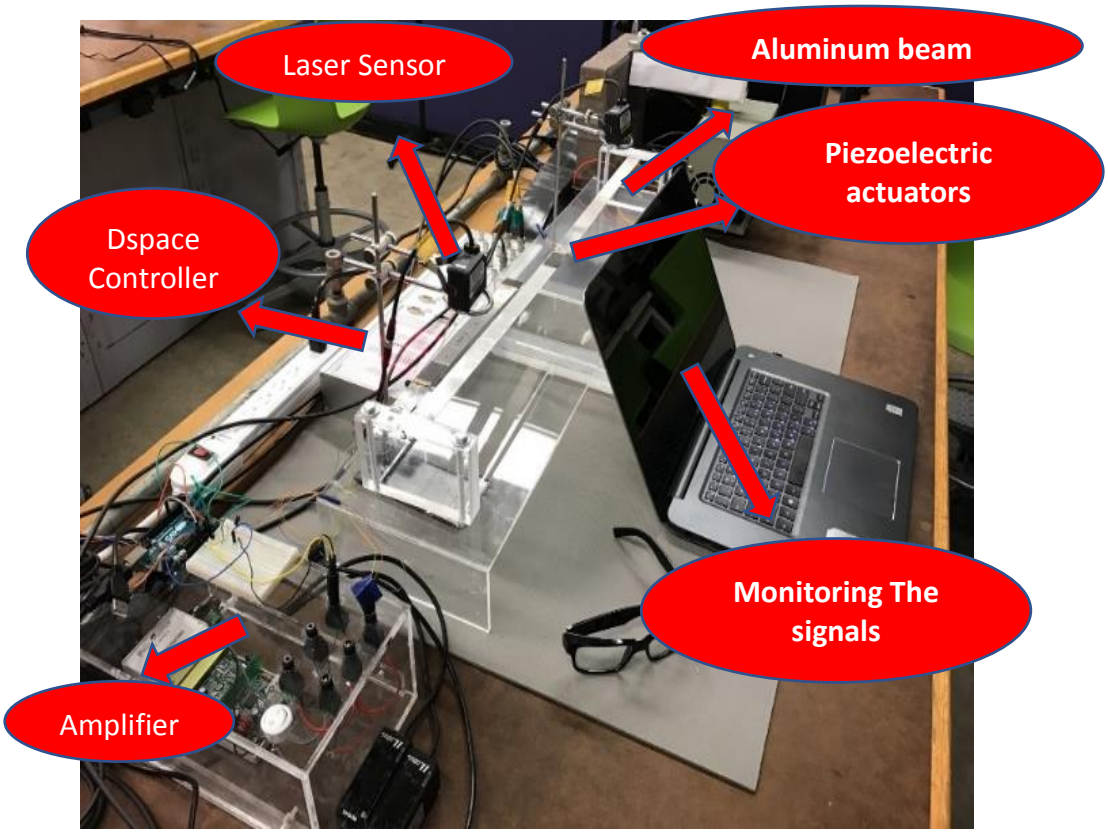

Figure 2 - The smart beam experimental setup in Lab E135 at San Jose State University.

The mechanical structure comprises a flexible aluminum beam with fixed endpoints. The aluminum beam is held transversal and clamped with screws and nuts from the sides. The piezoelectric actuator patches are attached on top of the beam. The laser sensor measures the vertical displacement of the beam at a particular point around the middle of the beam.

The beam and other components are designed in, Creo Parametric, a CAD software. Figures 4, 5, and 6 are the modeled beam in the software with the real dimensions. figure 4 shows the model from the top view where the laser sensor emits the laser light. Piezoelectric actuators are also modeled in Creo Parametric. Figure 5 shows the cross section of the beam from the front view. In this view the thickness of the beam is shown separated from the thickness of the actuator. In Figure 6, the isometric view of the beam is

presented where the piezoelectric patches are bonded to it.

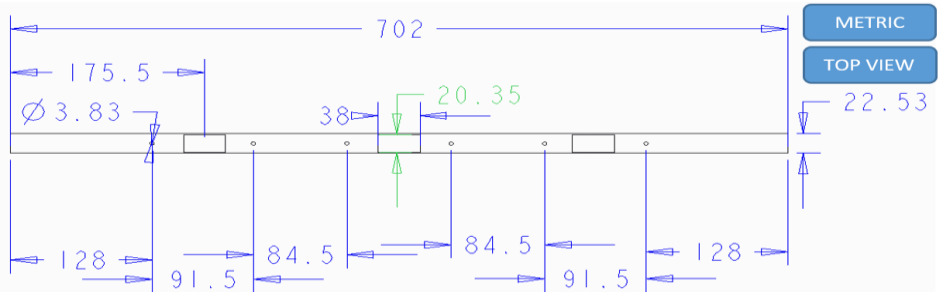

Figure 3 - Top-view of the experimental beam.

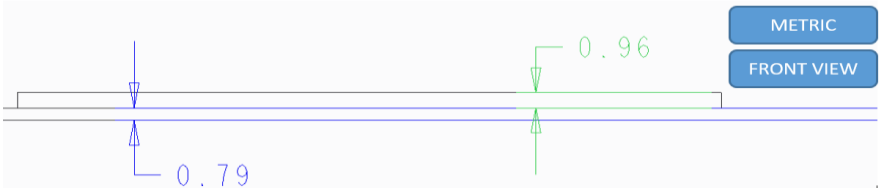

Figure 4 - From the view of the experiment beam (partial view).

Figure 5 - isometric view of the beam integrated with the piezoelectric actuators.

2.2 Piezoelectric System

Piezoelectric actuators are one of the most well-known actuators for active vibration control. They have the capability of bending because of applying a voltage to

them. The piezoelectric patches can also be used to measure displacement by getting deflected and generating a voltage corresponding to the input. In this project, piezoelectric actuator systems are used for two main purposes: First, to serve as an actuator, and second, to serve as a disturbance source. In both cases, the input of the system is voltage, and the output is displacement. The range of excitation frequency of piezoelectric actuators is from 0 Hz to 10 kHz, and the legitimate voltage range is from -110 to 110 v.

The specifications of the piezoelectric actuators are provided by the PiezoMaster company. The information shown in Table 1 is useful in the calculation of the force applied to the beam analytically. The total deflection and the blocking force are the functions of the voltage input. The total deflection is given in [mm], the blocking force in [N] and the resonant mode in [Hz].

Table 1 - manufactured information of the piezoelectric actuators.

Characteristic	Calculation	Result
Total Deflection	2.2E-6 ($[l_f]^2$ / $[h]^2$) ([V])	mm
Compliance	26.4E-5 $[l_f]^3$/ ([w]) $([h]^3)$	--
Blocking Force	[deflection] / [compliance]	N
Resonance Frequency	3.2 x 10^5x ([h] / $[l_f]^2$)	Hz

2.3 Amplifier

The purpose of using an amplifier in the system is to magnify the voltage input. The amplifier used in this project has three channels enabling it to receive three input signals and after the amplification process release, three amplified signals for the two above mentioned piezoelectric actuators. The system receives a discretized signal from the digital controller and increases it 20 times. In this project, the piezoelectric actuators can be energized from -100 v to 100 v. The amplifier is getting the input of 5 volts from the dSPACE controller board, and after amplification, the actuators are supplied by 100 v. However, for safety protection, the dSPACE controller is set to saturate the signal at 80 v.

The bandwidth of the Amplifier is 20 kHz. Then, in the frequency range that the dSPACE controller board is working, 100 Hz, the effect of the amplifier dynamics can be neglected.

2.4 Digital Controller Device

An experimental testbed acquired a unit of control. A unit of control is a domain where all signals would acquire into control unit or depart from the control unit. The process of correction of the signal takes place via the complex electronics' system which is defined in the controller. The signal is presented in two different forms of analog or digital. However, the digital controller can only process the digital or discretized signal [30]. There are two pieces of equipment, ADC, and DAC which solve this problem.

Some of the digital controllers contain ADC or DAC built-in. The Digital controllers are widely used in the application of closed-loop systems. The first digital computer is used in 1940 [31]. Many controllers developed since then, and the price of the controllers has dramatically dropped over the time.

The dSPACE controller board is used to control the beam in this project. The controller sampling can handle up to 10 kHz. The built-in 16-bit DAC is one of the useful features of the controller. The block diagram which is designed in SIMULINK is implanted in dSPACE controller board. The dSPACE controller is connected to the sensor via BNC cable.

A single sensor is used to pick up the vertical displacement of a point about the middle of the beam. The laser sensor detects the movement with 3.3 kHz sampling rate, i.e. the device will pick up 3300 samples of displacement per second with an accuracy of a micrometer.

2.5 Software

Two softwares are used in this project as the user interface to collect the data, process the data, and implement the controller: MATLAB/SIMULINK and ControlDesk. Matlab has the simulation environment or virtual environment. On the other hand,

ControlDesk is the software to store and display the experimental data. In control desk, the user is able to customize the number of inputs and outputs. ControlDesk directly obtains the information from the MATLAB/SIMULINK. Any parameter that is defined in the SIMULINK environment can be called in the ControlDesk for further investigation.

3.0 DATA ACQUISITION

After completing the experimental setup, designing the desired controller is pursued which satisfies all the stability margins and design targets. To desing the controller finding the plant model transfer function is a key factor. The advantage of acquiring the plant is that the control designers can develop and try as many controllers as desired in the simulation environment. After finding the optimized solution, they can implement the controller in the system for final validations in practice. The Data-driven method outperforms other methods, such as fitting a high-order transfer function using system identification, because it is counted as the actual plant model rather than an approximation of it.

3.1 Characterizing the Plant

Figure 3 presents the process of data collection to find the frequency response of the smart clamped-clamped beam. The laser sensor is located right next to the middle of the beam. The sensor is picking the vertical displacement of the beam. The data is transferred via the BNC cables to the control unit, dSPACE. The control unit is versatile. For data acquisition, the control unit saves data and sends the actuating signal toward the amplifier and the middle actuator. The middle actuator excites the beam. By doing so a transfer function from point A to point B is obtained.

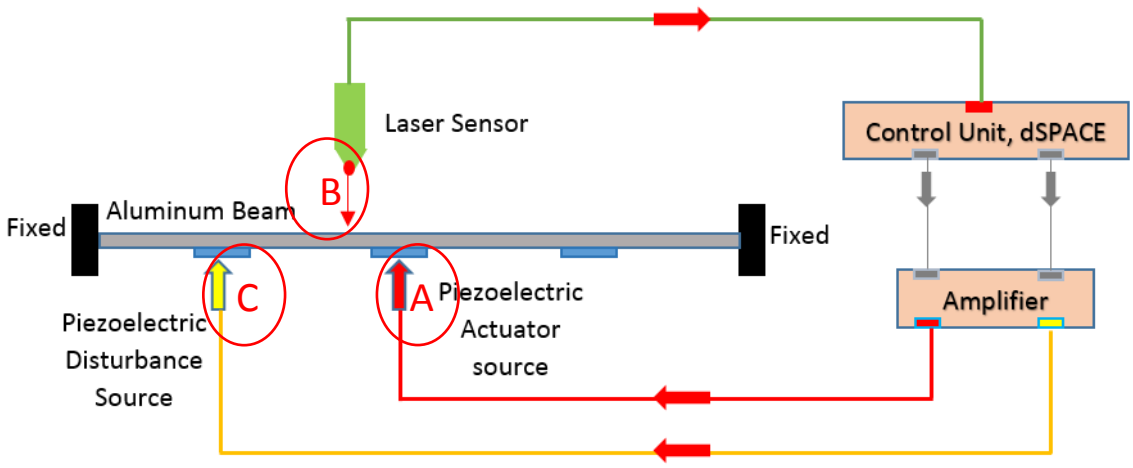

Figure 6 - The setup configuration consists of mechanical components.

Different sinusoidal input signals are imposed on the system and outputs are collected. Because the steady-state response of an LTI system is linear with the same frequency of the excitation, the output can be collected as a set of frequency vector, initial amplitude vector, and response vector. Using MATLAB's "frd" function, the system can be analyzed as a numerical non-parametric model for frequency domain control system analysis.

3.2 Vibration Suppression Technique

To suppress the vibration of the clamed-clamped beam, which is the goal of the study, it is reasonable to pick only one point over the beam to be suppressed. Reduction of the vibration at point B would cause reduction of vibration at the entire of the beam except for the points that are in the vibration nodes. An example of a node is when the system vibrates in the second mode. In that case, the node would be created in the middle of the beam. If the sensor placed right on the node point, then it will not be able to read the displacement. Knowing the fact, the laser is placed at a point with distance from the center. With that, the data is collected from the input point A to the output point B. Using the data, a frequency response data can be collected from the input voltage to the

displacement output.

3.3 Beam Excitation

In order to find the transfer function from point A, where the actuator is, to point B, where the laser is located, a set of input and output data is needed. The input set is desired to be harmonic to obtain the frequency response plot of the system. To create the harmonic input excitation MATLAB and SIMULINK are used as shown in Figure 7.

The time is the independent variable for the function above. The $\boldsymbol{f1}$ function is defined in the SIMULINK environment to create the time as an independent variable and returns the discretized output signals which will be used as the frequencies of the input signal. As depicted above, the function is getting the $T_{actvive}$ as the time that the system is on, $T_{deactive}$ as the time that the system is off and $Freq_{step}$ as the stepped frequency which is increasing the frequency in every step. In this experiment, $T_{deactive}$ = 2 s, T_{active} = 8 s, and the $Freq_{step}$ = 0.25 Hz were used. The $\boldsymbol{f2 = sin(2\pi ft)}$ function is as simple as a sinusoidal function where it receives time and the discretized frequency, and returns the incremented sinusoidal which turns on and off repeatedly, as depicted in the right corner of Fig. 7.

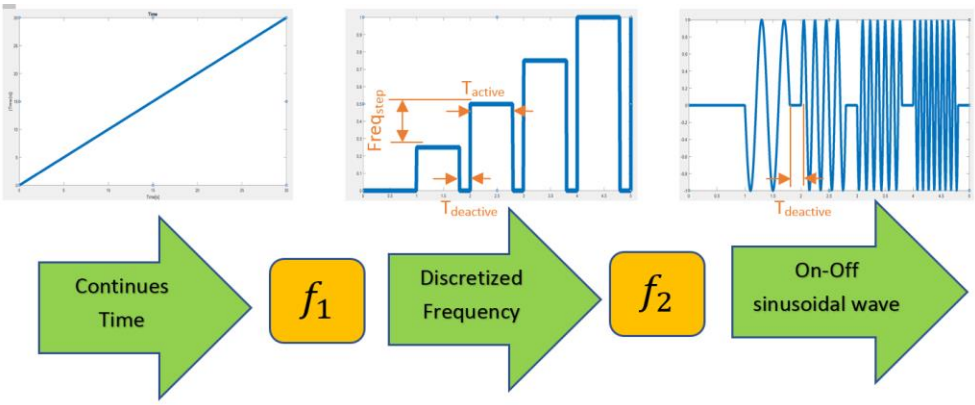

Figure 7 - The SIMULINK process in discretizing the frequency and generating sine waves.

The time signal vector is [0, 0.001, 0.002, 0.003, 0.004, …, 20000], where the last

data is picked at the time of 20000 seconds is equivalent to 5 hours and 33 minutes. The frequency vector in Hz is [0, 0.25, 0.5, 0.75, 1, …, 500]. The final value is chosen to be 500 Hz because the sampling time is 0.001 s, i.e. the sampling rate is 1000 Hz. The information above 500 Hz is not used in this test experiment.

The final sinusoidal wave passes through a block diagram of a digital to analog converter, (DAC) after passing through proper amplitude conversions that dSPACE controller board is required. On the other side, the laser sensor is able to pick up data with 3300 Hz sampling rate as an analog signal between -5 v to 5 v. Then, the analog signal passes through a 16-bit ADC to the block diagram of digital converter and multiplied by a proper gain which is required for the dSPACE controller board the setting of the SIMULINK is set for fixed time step of 0.001s. Then the computational process on the the dSPACE controller board will be based on the fixed time step. The solver of the internal simulation is chosen ODE5. dSPACE has built-in digital to analog converter (DAC) and analog to digital converter (ADC). For taking the advantages of these Block diagrams, the SIMULINK file must be uploaded on the dSPACE digital processor.

3.4. Running the Testbed

After the SIMULINK section to collect the data is completed, the next step is to implement it in the dSPACE controller board MATLAB SIMULINK is provided this feature by just choosing dSPACE as an external hardware and click to connect all data to the digital processor's memory. The ControlDesk is letting the user to directly observe the input and outputs in different forms such as bar, plot, or display.

The software has another feature to save desired data. Recalling that the FRD object in MATLAB is required 3 inputs: the frequency spectrum, the complex form of output over input, and the sampling time. To obtain the complex form of output and input, the ControlDesk must record both outputs from the sensor, input which is generated by the processor, the independent variable of time, and discretized frequency. Then, all the data are saved in a consolidated .mat file to be loaded in the MATLAB

4.0 DATA-DRIVEN SYSTEM IDENTIFICATION

By the set of inputs and outputs, the system can be characterized as it was discussed earlier. The data of input and output which are collected in the previous step now is used to characterize the plant. There are some methods to facilitate this conversion such as using Fast Fourier Transform (FFT) and Data Marching using LTI feature. In this project, Data-Matching is used because of the white noise in the entire of the spectrum as depicted in Figure 8. The method of FFT is useful when the signal to noise ratio (SNR) is small. See appendix for the details of FFT technique.

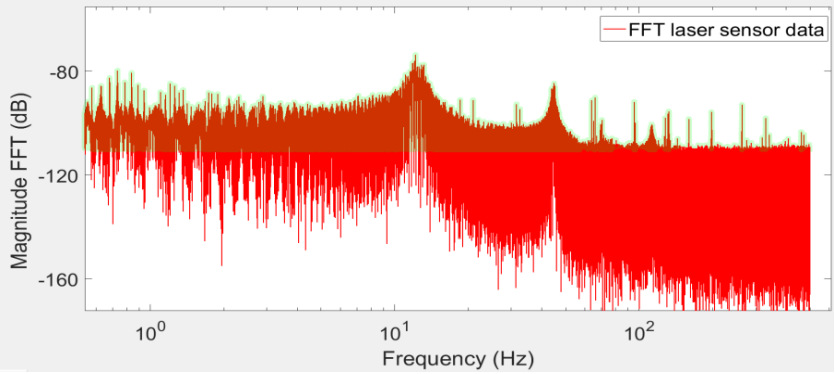

Figure 8 - Fast-Fourier-Transform frequency response data of the plant.

In order to use the method of LTI system data matching the system the collected time data is imported for further calculations. Figure 9 shows the LTI system behavior. If the system is excited with a sinusoidal signal, then the output of the system is another sinusoidal function in the steady state condition. To characterize the beam, a number of sinusoidal excitation signals within a certain frequency interval are needed to obtain the frequency response data (FRD) of the system.

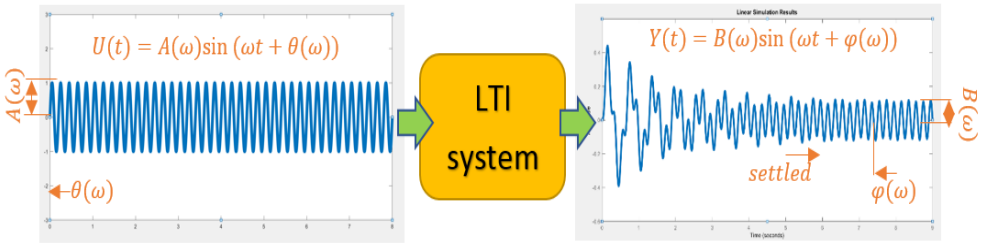

Figure 9 - The linear time invariant behavior.

4.1 Data Matching Method

In this process, the collected data is loaded into the MATLAB workspace. To get the data-driven complex transfer function, the amplitude of the input voltage signal is known, and the phase delay is set to zero. However, the output signal must be calculated through the process of data-matching. To fit the sine function to get the amplitude and phase, there are plenty of data in the 8 s which the system is energized in every frequency step. To avoid the transient part of the response, the sine function is fit to only the last two cycles of the response. The time duration of the last two cycles vary, depending on the frequency of signal, as shown in Figure 10.

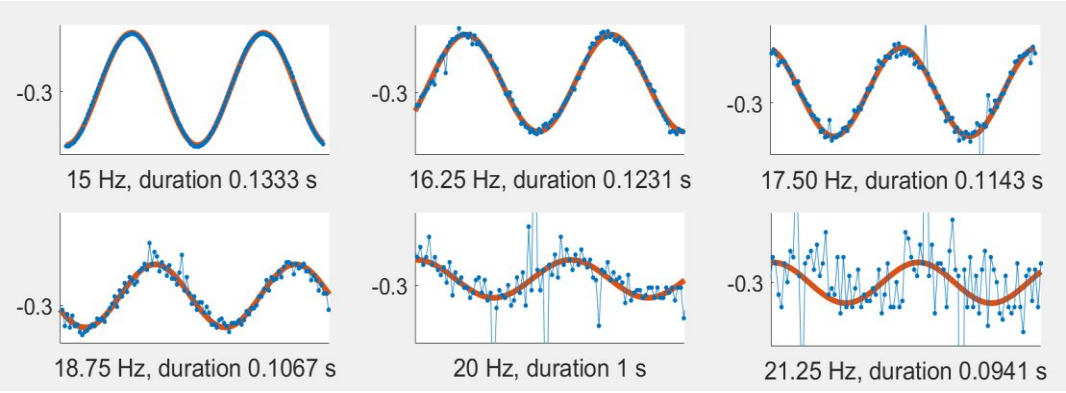

Figure 10 - Fitting a sine function (red line) to the sensor data (blue line).

This process is iterated for 2000 times at every excitation frequency within 0.25 Hz to 500 Hz. For example, in the interval between 15 Hz and 16 Hz the frequency samples are:15 Hz, 15.25 Hz, 15.5 Hz, 15.75 Hz, and 16 Hz.

The function used for fitting experimentally collected data is $\boldsymbol{f(\omega) = B(\omega)sin(\omega t + \phi(\omega)) + bias(\omega)}$. The equation contains three variables to be found for every frequency step: $\boldsymbol{B(\omega), A(\omega), bias(\omega)}$. Assuming that the excitation frequency is the same as the output frequency of the system, then the $\boldsymbol{\omega}$ becomes a known variable. Using $\boldsymbol{B(\omega)}$ and and $\boldsymbol{A(\omega)}$ the amplitude of the input and the amplitude ratio, the magnitude graph can be obtained. By using $\boldsymbol{\varphi(\omega)}$, and the and phase of the input, which in this study is zero, the output phase graph can be obtained. Note that the phase is wrapped between $\mathbf{0}$ and $2\boldsymbol{\pi}$. The amplitude ratio and the phase are calculated based on:

$$G(j\omega) = \frac{Y(j\omega)}{U(j\omega)} = \frac{B(\omega)e^{j\varphi(\omega)}}{A(\omega)e^{j\theta(\omega)}}$$

$$|G(j\omega)| = \left|\frac{B(\omega)}{A(\omega)}\right|$$

$$\angle\, G(j\omega) = \varphi(\omega) - \theta(\omega) \qquad (1)$$

By collecting enough data from a range of frequency, the amplitude and the phase of the system for every single frequency are obtained. i.e. every frequency has a corresponding amplitude ratio, phase delay, and a bias shift. Using the set of amplitudes and the phases, frequency response plot is obtained as shown in Figure 8.

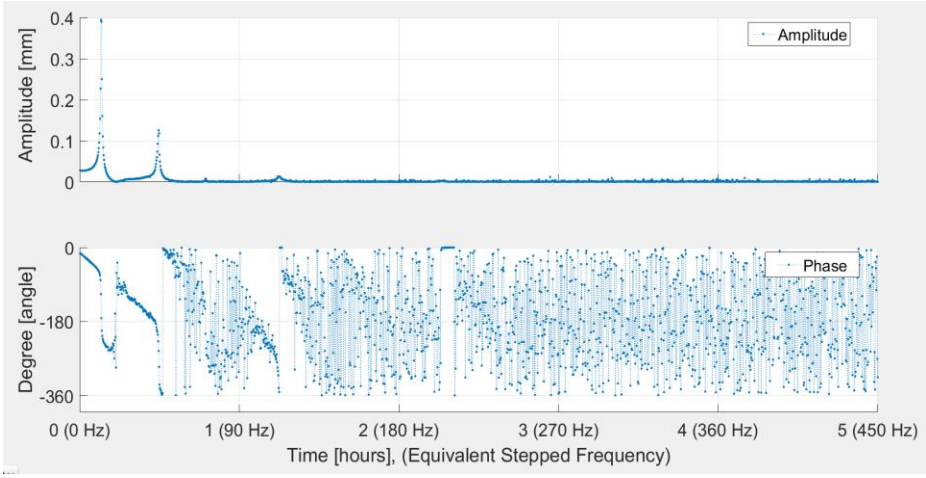

Figure 10 - Amplitude and phase response of the system using the sine function fitting method.

Using the third term, $\boldsymbol{bias}(\boldsymbol{\omega})$, The graph can be adjusted to the new position as show in Figure 11. The red data is the raw response of the system. The blue response is the adjusted response which is aligned in the vicinity of zero.

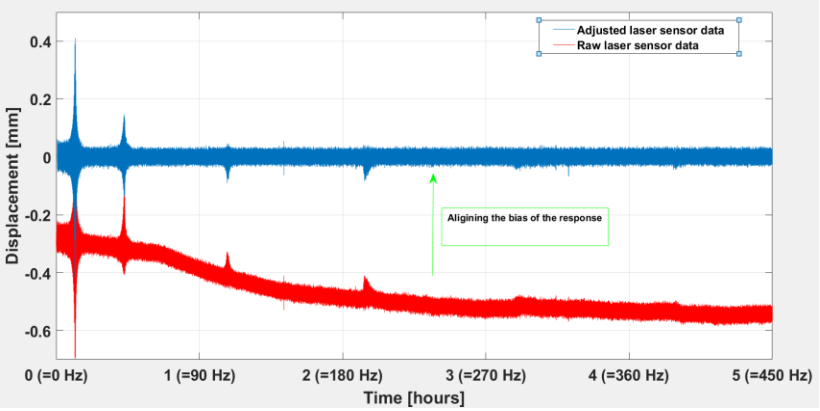

Figure 11 - Aligning the sensor's data around zero using the bias set data.

Finally, to obtain the transfer function and to move to control-design section, the $\boldsymbol{frd}$ command of MATLAB is used. The function $\boldsymbol{frd}$ requires response vector which is the sensor's output, the excitation input, which is the voltage to the actuators the frequency vector, and the sampling time. The output of the $\boldsymbol{frd}$ MATLAB function is a set of MATLAB defined cells. The FRD object in MATLAB behaves like a discretized system with some limitation. For example, the system cannot simulate and yield the response of the system for any input.

Figure 12 shows, the FRD Bode diagram is shown. The upper plot is the Magnitude of the transfer function, and the lower plot is the phase of the function. However, there are some limitations to using the FRD system in control system design process, but using this system provides the information to analyze and plot the response of the Open-loop transfer, Closed-loop and Error transfer function.

The FRD system in MATLAB is defined with 18 parameters such as Response, IO Delay, Input Delay, sampling time, Frequency, and frequency unit. The most important labels are the complex response and the set of frequencies.

The phase margin is the difference between the value of the phase from -180 when Bode plot of Open-loop transfer function crosses zero dB. Then as the phase of the system is unexpected and it possible to pass -180, the controller must be designed in a way that the Open-loop transfer functions' Bode plot, for all 6 plants, do not cross the 0 dB except at the bandwidth. As the safety factor, the Open-loop transfer function was kept below 10 dB in the higher frequencies.

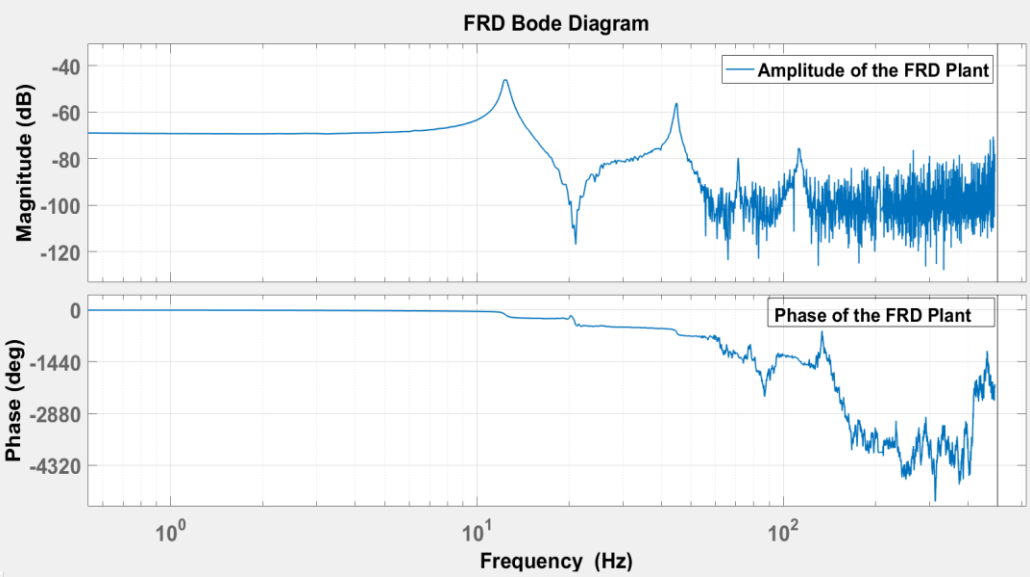

Figure 12 - Bode Plot of the data-driven modeling of the beam.

4.2 Collection of a set of plants

It is desired to design a robust controller. To design a robust controller a set of different plants must be provided to ensure the control system design can function well even in different circumstances. Different holes are drilled into the beam to mount weight to it as shown in Figure 13.

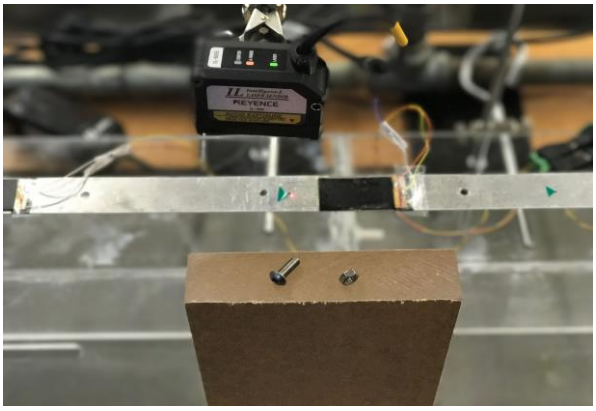

Figure 13 - A screw and a nut to increase the weight of the beam changing the plant.

By adding weight to the system in a different location of the beam, six different plants are collected each one with a different color. The natural frequencies of the first, second, and the third mode are tightly close to each other. The dc gain of all plants are adjusted based on the average of the all six dc-gains.

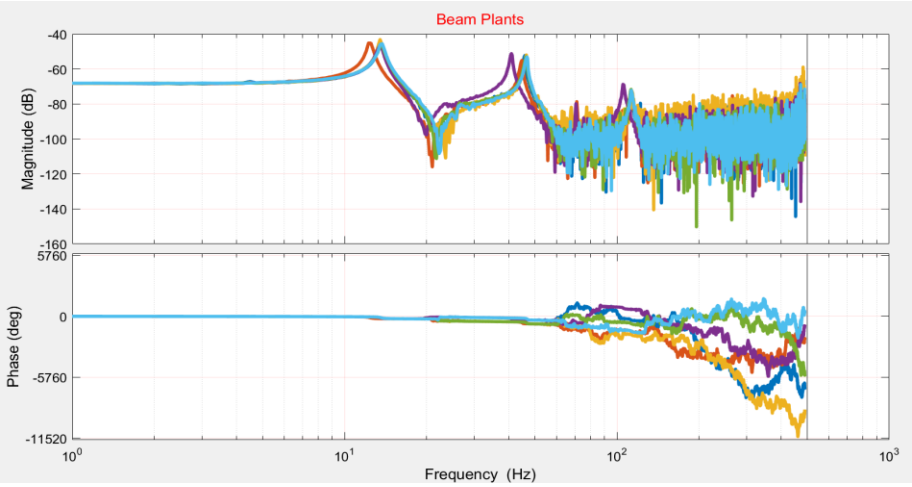

Figure 14 - a set of six different plant models of the clamped-clamped beam

5.0 DATA-DRIVEN ROBUST CONTROL OPTIMIZATION

The goal of the control optimization function is to receive a controller with manually tuned parameters as well as constraints as inputs and returns a controller with

optimized parameters as an output. the controller structure is a transfer function that is the cascade of PI-controller, low-pass filter, and a set of notch filters. The controller transfer function is designed to be dependent on eighteen parameters. These variables are iterated using a numerical optimization algorithm to yield the minimized cost function. The cost function is calculated using a quadratic formula based on a set of design's objectives such as stability margins, and performance. The last controller with optimized parameters will be used to control the smart beam's vibration.

5.1 Controller Configuration

The controller structure consists of a PI-controller, a low-pass filter, and a set of notch filters as shown in Equation 2. The controller is initially designed in the Laplace domain and then is discretized by transferring into the z-domain where the z-domain transfer function is used for the optimization.

$$Controller[s] = PI_{Controller}[s] * lowPass_{filter}[s] * Notch_{filter}[s] \quad (2)$$

In Equation 2, the proportional-integral controller, $PI_{Controller}$, is the first controller's element where its structure is shown in Equation 3. The controller has two parameters, k_p and k_i

$$\boldsymbol{PI_{controller}[s] = \left(k_p + \frac{k_i}{s}\right)} \quad (3)$$

The k_p is the proportional term which largely affects the higher frequency region in the frequency response plot (Bode plot). The k_i is the integral term which mostly impacts the lower frequency region and makes the steady-state error to be zero. Then, using a combination of the both elements provides a functional balance for the entire of the frequency spectrum.

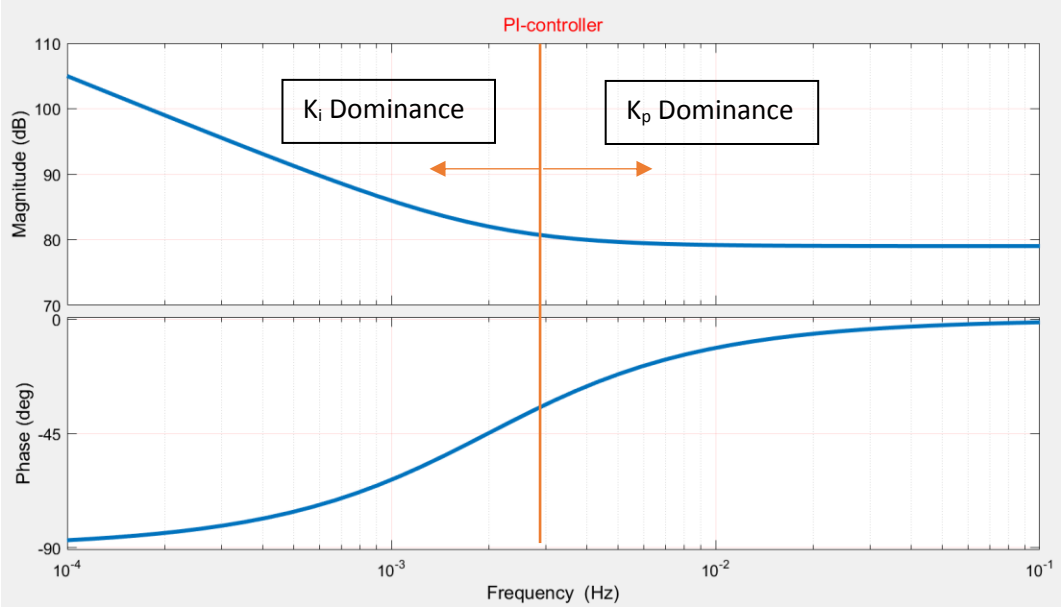

Figure 15 - Bode plot of the PI-Controller that used in the controller.

In Equation 2, the controller's second element is a low-pass filter. A low-pass filter is comprised of a DC gain and a cut-off frequency. A low-pass frequency would pass low-frequency signals and attenuate high-frequency signals. A low-pass filter is constant at first with a certain DC gain, then will start decaying 20 dB per decade when passes the corner frequency. The low-pass filter has 90 degree phase delay in the final value.

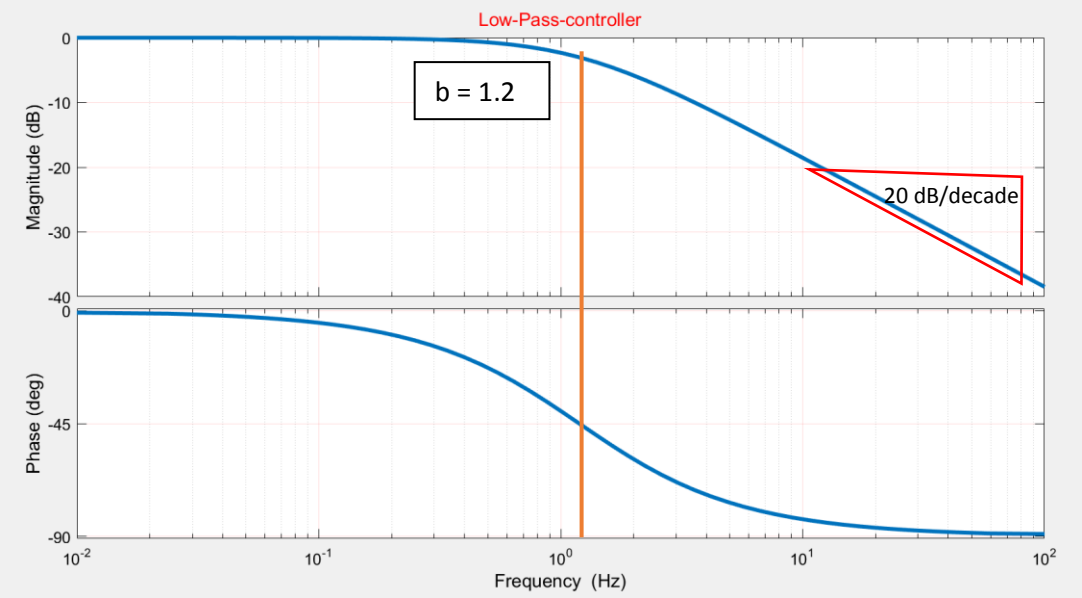

Figure 16 - Bode plot of Low-Pass filter that used in the controller

In Equation 2, the controller's third element is a set of notch filters. Notch filter has four variables as shown in Equation 4. The key factor is the damping ratio of the denominator is always greater than the numerator. The notch filter's equation as it can be seen from the Bode plot of the notch filter, in Figure 17, a notch filter's transfer function can be reconstructed based on frequency, depth, and width of the notch.

$$\boldsymbol{Notch_{filter}[s]} = \left(\frac{\boldsymbol{s^2+2\xi_N\omega_N+\omega_N^2}}{\boldsymbol{s^2+2\xi_D\omega_D+\omega_D^2}}\right) ; \boldsymbol{\xi_D > \xi_N} \qquad (4)$$

Figure 17 shows Bode of a notch filter where the frequency of occurrence attenuations is at13 Hz. As an advantage of a notch filter, the amplitude ratio and the phase delay, everywhere except the vicinity of notch frequency, is neutral.

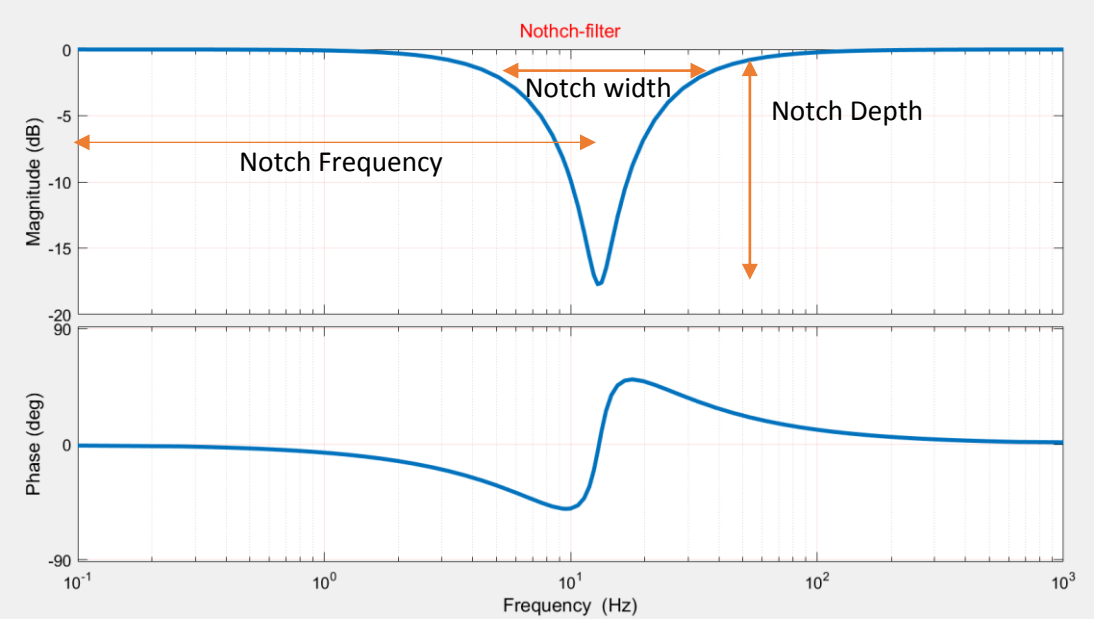

Figure 17 - Bode plot of Notch-Filter that is used in the controller.

Equation 5 presents a cascade of 5 notch filters. As discussed, each notch filter has three variables: frequency, depth, and width. Then the combination of all five notches, have fifteen variables in total. Figure 18 is the Bode plot of the all five notch-filters together. The frequency variable of each notch filter corresponds to the resonant frequencies of the plant. The depth and width of each notch vary depending on the shape and magnitude of

the resonant modes.

$$\boldsymbol{ConvolutedNotch_{filter}[s]} = \prod_{i=1}^{5}\left(\frac{s^2+2\xi_{Ni}\omega_{Ni}+\omega_{Ni}^2}{s^2+2\xi_{Di}\omega_{Di}+\omega_{Di}^2}\right) \; ; \; \xi_D > \xi_N \qquad (5)$$

Equation 6 presents a cascade of the three transfer functions, the PI-controller, the low-pass filter, the set of notch-filters.

$$\boldsymbol{Controller[s]} = \left(k_p + \frac{k_i}{s}\right)\left(\frac{b}{s+b}\right)\prod_{i=1}^{5}\left(\frac{s^2+2\xi_{Ni}\omega_{Ni}+\omega_{Ni}^2}{s^2+2\xi_{Di}\omega_{Di}+\omega_{Di}^2}\right) \; ; \; \xi_D > \xi_N \qquad (6)$$

$$Controller[s] = \frac{\begin{array}{c}96000\ s^{11} + 9.55e06\ s^{10} + 7.114e10\ s^9 + 6.138e12\ s^8 + 1.017e16\ s^7 + 6.932e17\ s\text{^}6 \\ + 4.632e20\ s\text{^}5 + 2.23e22\ s\text{^}4 + 5.291e24\ s\text{^}3 + 1.239e26\ s\text{^}2 + 1.583e28\ s + 1.319e26\end{array}}{\begin{array}{c}s^{12} + 322.2\ s^{11} + 7.757e05\ s^{10} + 2.234e08\ s^9 + 1.278e11\ s^8 + 2.73e13\ s^7 \\ + 6.798e15\ s^6 + 9.67e17\ s\text{^}5 + 9.755e19\ s\text{^}4 + 5.994e21\ s\text{^}3 + 2.071e23\ s\text{^}2 + 1.319e24\ s\end{array}} \qquad (7)$$

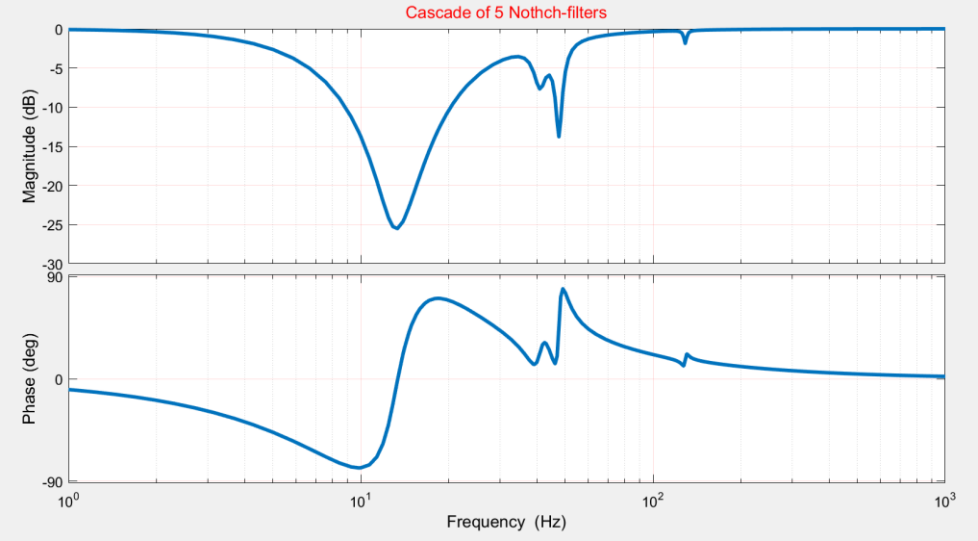

Figure 18 - Bode plot of all Notch-Filters together that used in the controller.

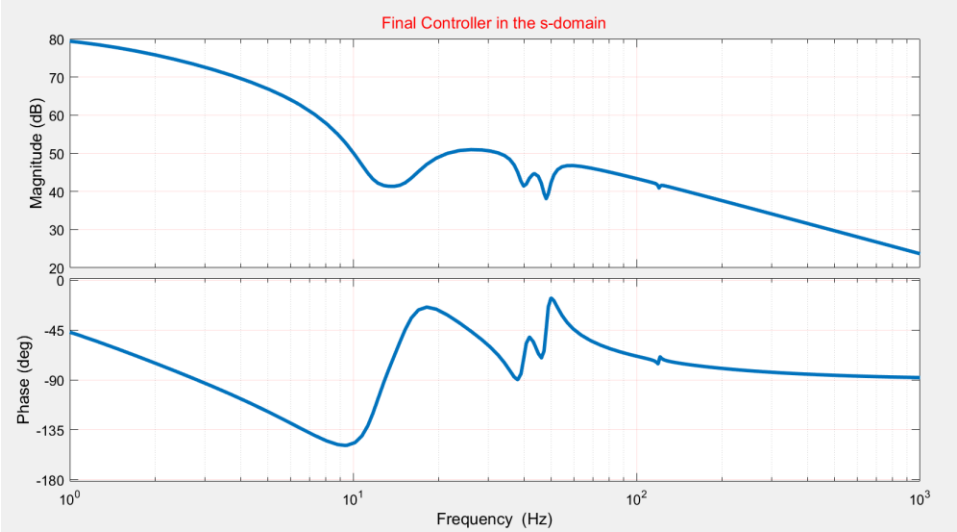

Figure 19 - Bode plot of the controller tuned manually.

Equation 7 is same as Equation 6, where all the variables are plugged numerically. As it can be seen from Equation 7, we have 12 poles and 11 zeros, based on the controller.

For implementation in the digital controller board, the controller in Equation 7 must be transferred to the z-domain. There are a couple of methods proposed in the literature such as zero-order hold, first-order hold, and pole-zero matching. In this study, the method of zero-order hold is used as a sample discretization scheme, as presented in Equation (8)

$$Controller[z] = (1 - z^{-1})G_{h0}\left(\frac{Controller\,[s]}{s}\right) \quad (8)$$

The corresponding command in MATLAB is as expressed by the Equation 9. Where the c2d stands for the continuous to the digital, the input is the controller in s-domain, the sampling time is 0.001 second, and the method is pole-zero-matched. The function of c2d is versatile, then for different application various methods can be utilized.

$$Controller[z] = c2d(Controller[s], T, 'zoh') \quad (9)$$

Equation 10 presents the controller equation in the z-domain:

$$Controller[z] = \frac{\begin{array}{c}85.91\,z^{11} - 875.9\,z^{10} + 4109\,z^{9} - 1.171e04\,z^{8} + 2.257e04\,z^{7} - 3.087e04\,z^{6} \\ + 3.059e04\,z^{5} - 2.197e04\,z^{4} + 1.12e04\,z^{3} - 3857\,z^{2} + 807.4\,z - 77.73\end{array}}{\begin{array}{c}z^{12} - 10.99\,z^{11} + 55.91\,z^{10} - 174.3\,z^{9} + 370.9\,z^{8} - 568\,z^{7} + 641.7\,z^{6} \\ - 539\,z^{5} + 334\,z^{4} - 148.8\,z^{3} + 45.24\,z^{2} - 8.418\,z + 0.7246\end{array}}$$

(10)

In Figure 20, the new controller is discretized and truncated after 500 Hz. Since the sampling frequency is 1000 Hz, the Nyquist frequency, which is half of the sampling frequency, becomes 500 Hz.

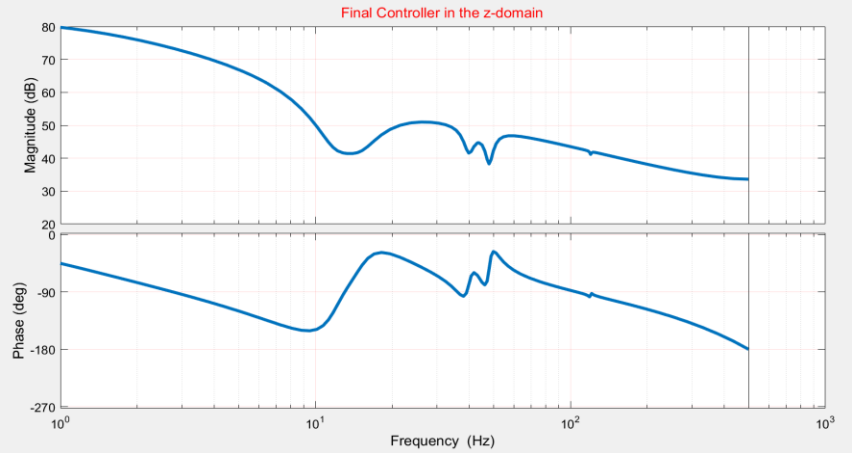

Figure 20 - Bode plot of the final controller in the z-domain with the sampling of Ts = 0.001.

5.2 Closed-Loop System Analysis

After finalizing the controller's structure, the controller's parameters are roughly chosen. The open-loop transfer function and error transfer function is studied every time. Then the controller parameters manually are shifted, and base on the error and trial method the best manually-tuned controller is found.

Equation 11 presents the open-loop transfer function, and Figure 21 shows the Bode plots of the manually-tuned controller for the 6 different beam's plants.

$$OpenLoop[z] = (Controller[z])(Plant[z]) \qquad (11)$$

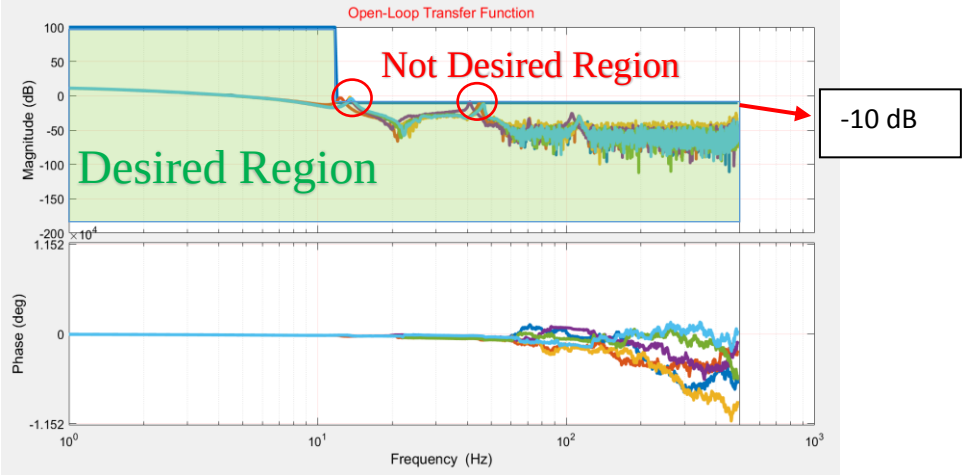

Figure 21 - Bode plot of the open loop transfer function in the z-domain.

The desired and undesired regions are shown in Figure 21. The open-loop is desired to cross the 0 dB only once and stays below -10 dB after the cross-over frequency. These safety factors are considered because it is possible for the phase margin to go below -180 degree and the system becomes unstable.

The error transfer function presents the transfer function from the reference r(t) to the error e(t). Equation 12 presents the error transfer function in the z-domain.

$$ETF[z] = \frac{1}{1 + Controller[z]Plant[z]} \qquad (12)$$

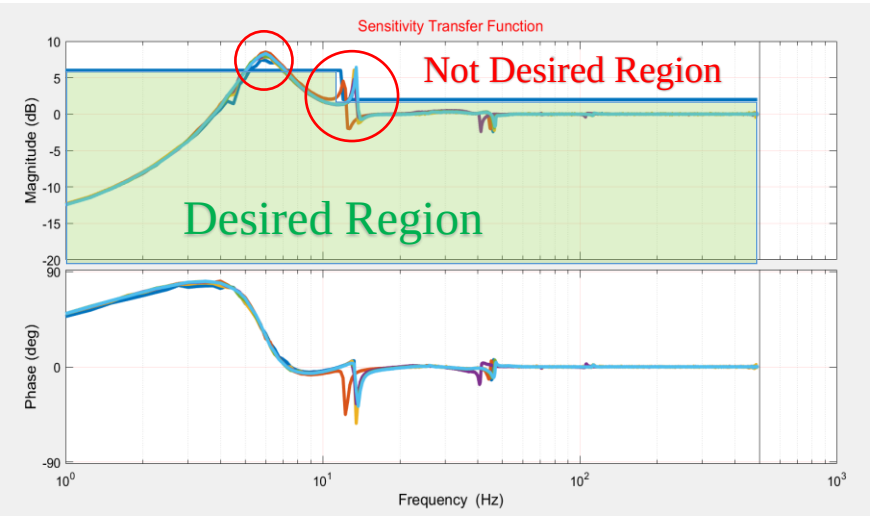

Figure 22 - Bode plot of the sensitivity transfer function in z-domain.

In Figure 22, the sensitivity (error) transfer-function is shown for the manual controller and the 6 plants. Two sets of thresholds are defined for the error transfer function: First for the frequency range below the first resonant mode, it is desired that the error magnitude does not go over than twice of the amplitude of the vibration, about 6 dB on the Bode plot. The second region is from 10 Hz onward. In this region, it is desired to keep the error below 2 dB. The regions that are circled in Figure 22 are responses that pass the threshold. The first one at the 4 Hz reaches 8 dB and the second one reaches 6 dB at the 13 Hz in the Bode plot.

The distribution of the stability margins for all the six open-loop transfer functions is shown in Figure 23. It contains the gain margin on the top, phase margin in between, and the bandwidth at the bottom. It is desired to shift the values toward the right side. By doing so, the system would be more stable and would have a better performance. However, there is a tradeoff between the stability and performance of the closed-loop controlled systems.

The values in Table 2 are obtained based on the open-loop and sensitivity transfer function frequency response data of the manually-tuned controller and the six plants. All values are shows the worst cases among all the plants.

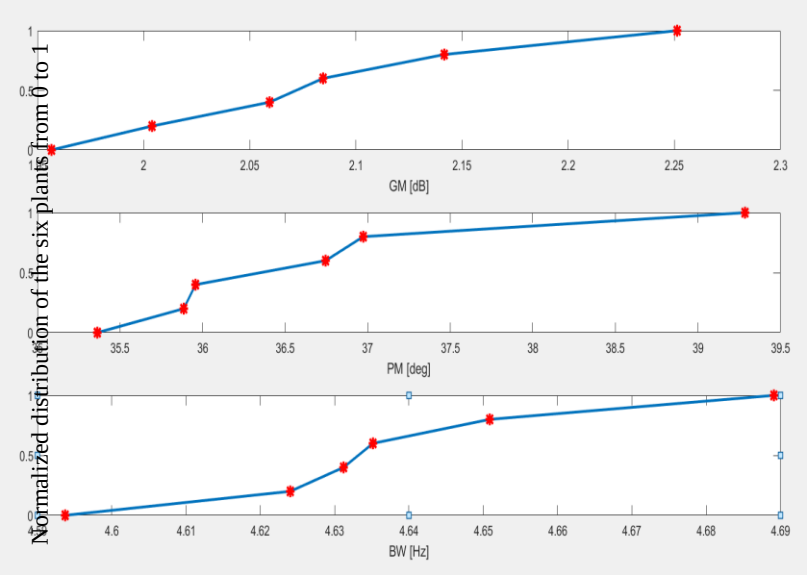

Figure 23 - plotting the gain margin, phase margin and bandwidth distribution corresponding to all the plants.

Table 2 - The exiting margins based on the initial manual-tuned controller.

Initial controller Margins		Values for all Plants
Gain Margin		(1.95-2.25) [dB]
Phase Margin		(35-40) [degree]
Bandwidth		(4.6-4.7) [Hz]
Sensitivity TF Maximum	0-12 Hz	8.52 [dB]
	12-500 Hz	6.43[dB]
Open-loop TF Maximum	0-12 Hz	11.2[dB]
	12-500 Hz	-3.4[dB]

5.3 Controller Objectives

A set of desired control objectives listed in Table 3 is pursued in work. Stability margins such as gain margin, phase margin, bandwidth must stay in certain ranges. Gain crossover frequency would be desired to be increased. The overall quality of sensitivity and open-loop transfer functions must be checked too.

Choosing desired values is challenging and needs to be characterized based on the empirical data or previous experimental results. The values must satisfy the properties of the closed-loop transfer function such as robustness and stability. Depending on the applications, these values could be different. For example, in the aircraft industry where human life is at stake, the stability margins must be chosen for a greater number to ensure the human safety. The chart above is inspired by the work of S. Bashash for HDD design [6]. Based on the paper, the bandwidth should be chosen around 10 percent of the Nyquist frequency to reject lower frequencies over a broader range. In sensitivity frequency response data, it is desired that the function stays below an upper bound to obtain a reasonable output results. The values of 0 to 12 Hz and 12 to 500 Hz are chosen as the different ranges of interest.

Table *3* - The desired margins and desired open loop and sensitivity.

Objective Function (f_k)		Desired Value	Weight
Min Gain Margin		3 [dB]	1
Min Phase Margin		40[degree]	1
Min Bandwidth		4[Hz]	1
Sensitivity TF upper-bound	0-12 Hz	6[dB]	10
	12-500 Hz	2[dB]	10
Open-loop TF upper-bound	0-12 Hz	100[dB]	10
	12-500 Hz	-10[dB]	10

5.4 Controller Optimization

The primary manual-tuned controller cannot entirely satisfy all the margins discussed in the previous section. The shortcoming of the manual tuning method is helping an objective could negatively impact other goals. For example, in sensitivity transfer function improving the lower-frequency can push the upper bound limit in higher frequencies or improving bandwidth might decrease the gain margin. Manual tuning the controller's variable is time-consuming in control design practice. Thus, developing an

automatic algorithm is needed to get the primary controller variables and returns the optimized ones. The control optimization process is shown in Fig. 24.

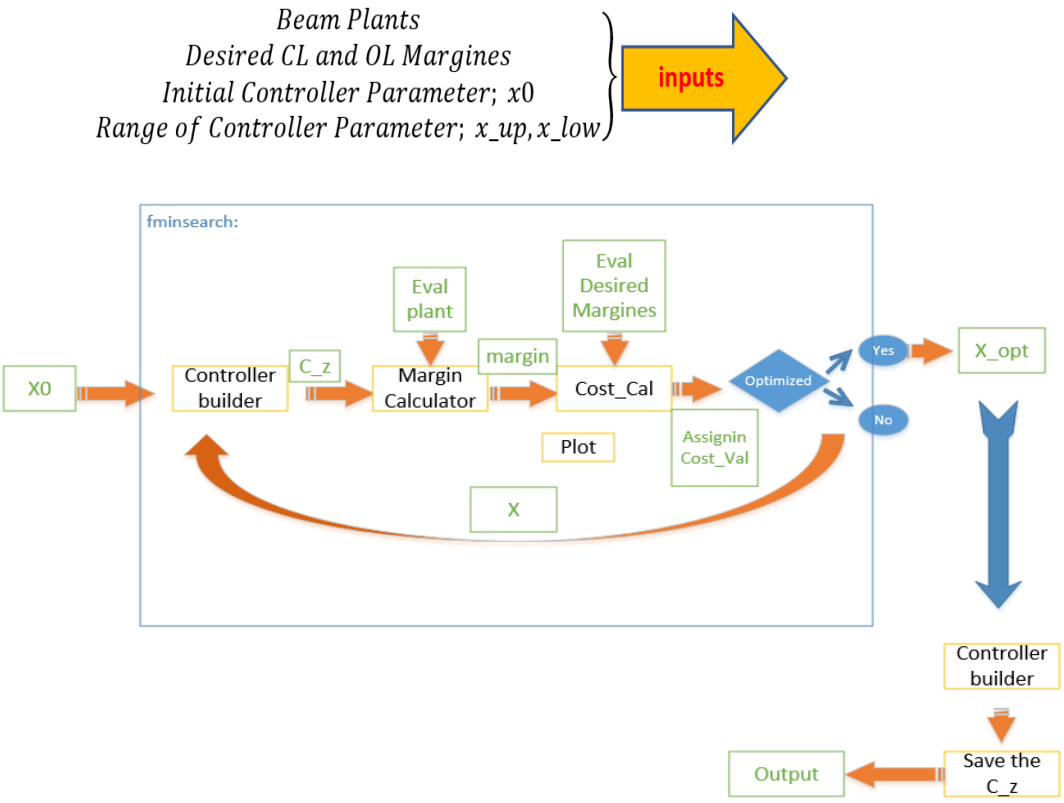

Figure 24 - The flow-chart of the optimization process.

5.5 Controller Optimization

In the process of controller optimization, there are 18 variables to be optimized as presented in Equation 13. These variables belong to the $PI_{controller}$, the low-pass filter and the sets of notch filters.

$$Controller[z] = f_{PI.Controller}[x_1, x_2] f_{Lowpass.filter}[x_3] \prod_{i=1}^{5} f_{Notch.fiter}[x_{3i+1}, x_{3i+2}, x_{3i+3}] \quad (13)$$

$$options = optimset('MaxFunEvals', 2000, 'Display', 'iter');$$
$$[x\_opt\ f\_opt] = fminsearch('cost\_at\_margins', x0, LB, UB, weight, options);$$

The function of PI-controller takes x(0) and x(1) relatively for kp and ki. The function of the low-pass filter is getting x(3) as the corner frequency of the low-pass filter. Notch parameters are not as straightforward as the other two controllers. To facilitate the process, another MATLAB function of Notch_builder is developed to get the three inputs of Depth [dB], Width[Hz], frequency[Hz].

As it is shown in the block diagram, every iteration process function of *controller_builder* is creating a controller in the z-domain where the input of the function is the set of the 18 x values.

5.6 Cost Function

The next step is to form the closed-loop system cost function based on the criteria discussed in the previous section. The cost calculator function is then used to compare the values of the target and the new controller-based values. The process is repeated until the final results are obtained. This process is done over and over to ensure the minimum cost is achieved. The formula of the *cost calculation* function is:

$$\begin{cases} w_k \left(\frac{f_k(q) - f_{desired,k}}{f_{desired,k}}\right)^2, & f_k(q) \geq f_{desired,k} \\ \varepsilon\left(f_k(q) - f_{desired,k}\right), & f_k(q) < f_{desired,k} \end{cases} \quad (14)$$

In Equation 14, w_k is the weight specified to each sub-cost and f_k is the calculated cost. $f_{desired}$ is the desired objective value. If the newly calculated target is less than the desired value, then, by a certain ratio factor of epsilon, it reduces the cost. By doing so, the system would know that the optimization track is correct.

The optimized cost value ends up landing at 0.2134 compared to the initial cost of 313.1123 for the manual tuned controller. The optimization results are shown in Figures 26, 27, and 28 which respectively depict sensitivity transfer function, open-loop transfer function and compared the distribution of the stability margins and the bandwidth.

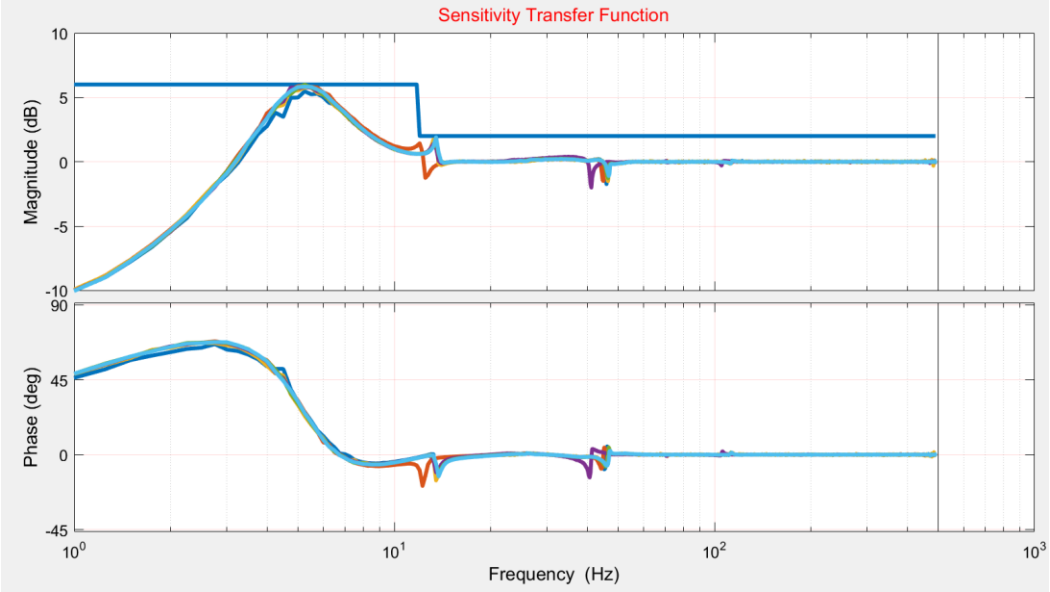

Figure 25 - Bode plot of the sensitivity transfer function in z-domain after optimization.

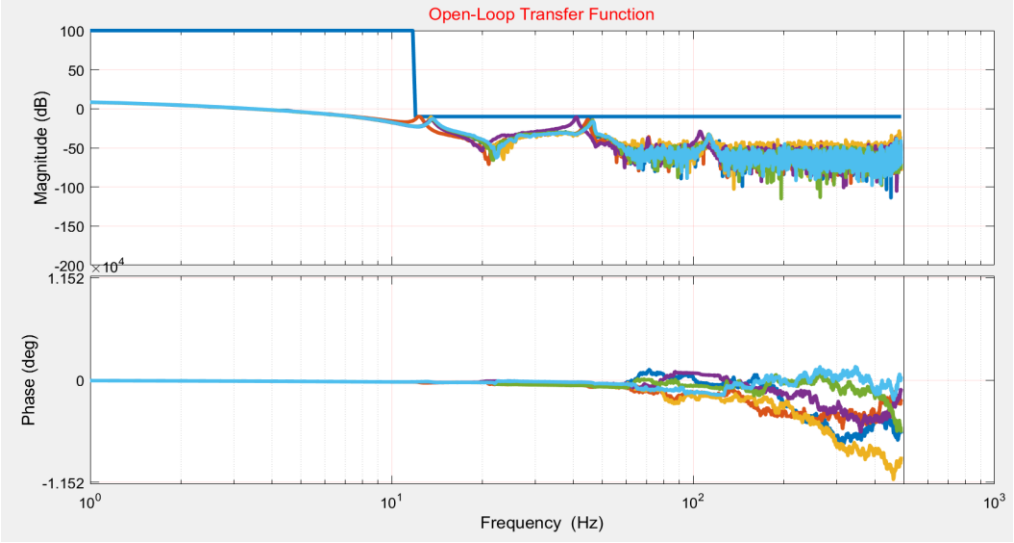

Figure 26 - Bode plot of the open loop transfer function in z-domain after optimization.

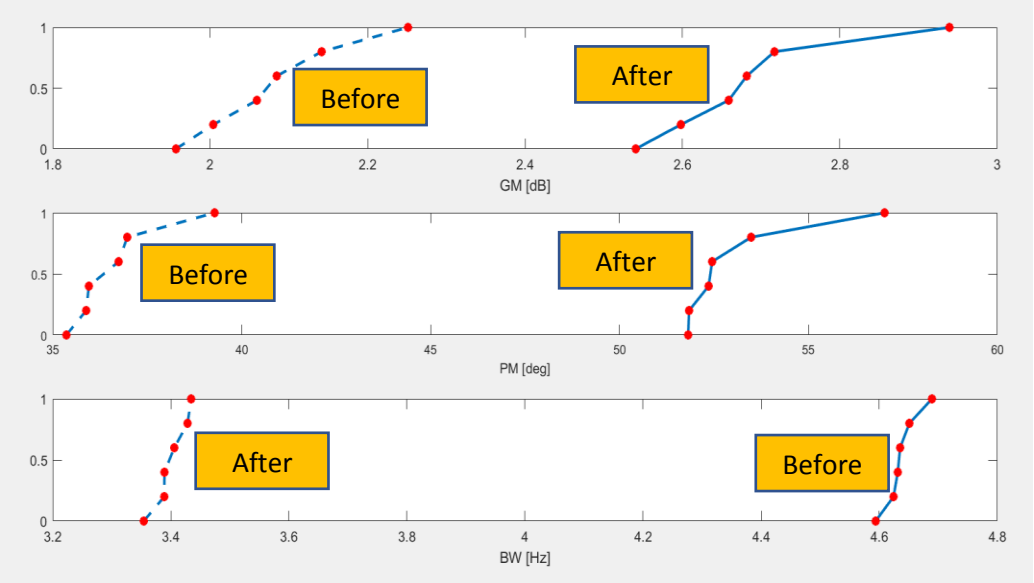

Figure 27 - Comparing the distribution of the gain margin, phase margin, and bandwidth.

As it can be seen in Figure 28, bandwidth of the system is reduced after optimization. However, the stability margins improve. As pointed out earlier, there is a tradeoff between the performance and stability of the closed-loop system.

6.0 RESULTS AND DISCUSSION

The final optimized controller is designed in the discretized form in z-domain. Then the controller is implemented in the real setup for the final evaluation of the controller and validation of the method.

6.1 Step Response

The response of the closed-loop system to step input is shown in Fig. 28. The system is able to react quickly to the step input and track it. Due to the creep effect of the piezoelectric actuator, however, the actuators depart from the reference signal after a

while due to the creep effect.

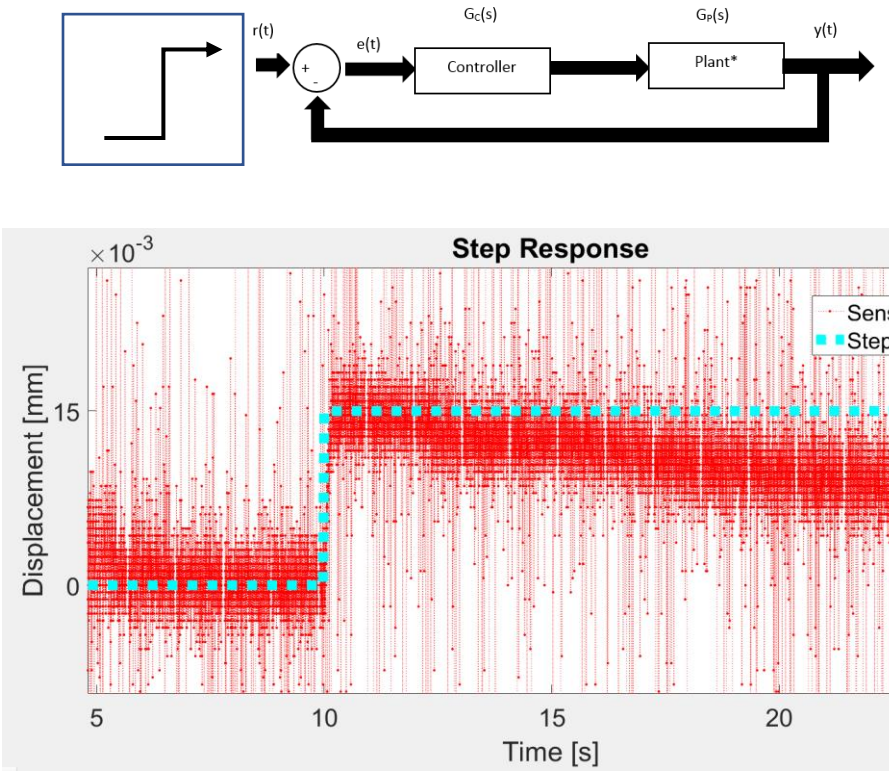

Figure 28 - The step reference r(t) and the response of the step y(t) plotted over each other.

6.2 Sinusoidal Reference Tracking

In this experiment, the reference of r(t) is chosen to be a sinusoidal function of the frequency of 2 Hz. As it can be seen from Figure 29 when the controller is OFF the beam is stationary, and the sensor is only picking noise with some bias. Once the controller is turned ON, after 10 seconds, then beam starts oscillating with the same frequency of the excitation and a reduction in amplitude and small phase shift.

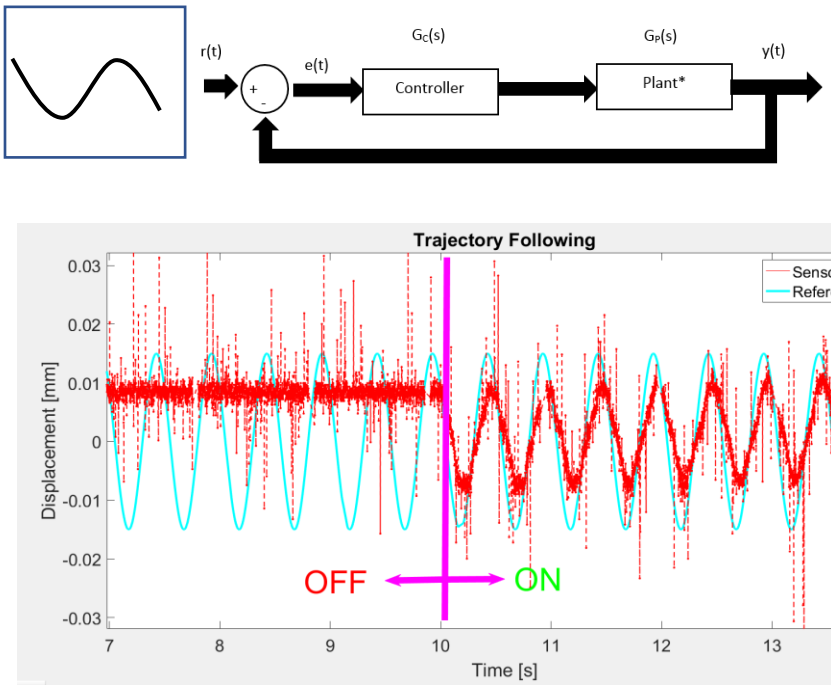

Figure 29 - The trajectory following for the ON-OFF controller, Blue line is a ref. r(t) and Red line is the response y(t) at 2 Hz.

6.3 Disturbance Rejection

In the disturbance rejection experiment (Fig. 30), the source of d(t) actively excites the system as the disturbance source. The reference r(t) is zero because the desired value of the system is to stay stationary even in the presence of the disturbances.

In Figures 31, 32, and 33, the graphs indicate that the response of the system has a close relation with the sensitivity transfer function. At some certain frequencies, the system has amplification of the disturbance, and at some frequencies, the system rejects the disturbance. For example, at the 0.5 Hz disturbance frequency, the error is minimized because of the integrator in the system. However, at 4 Hz the system reaches up to twice the open-loop error due to the peak of the sensitivity transfer function.

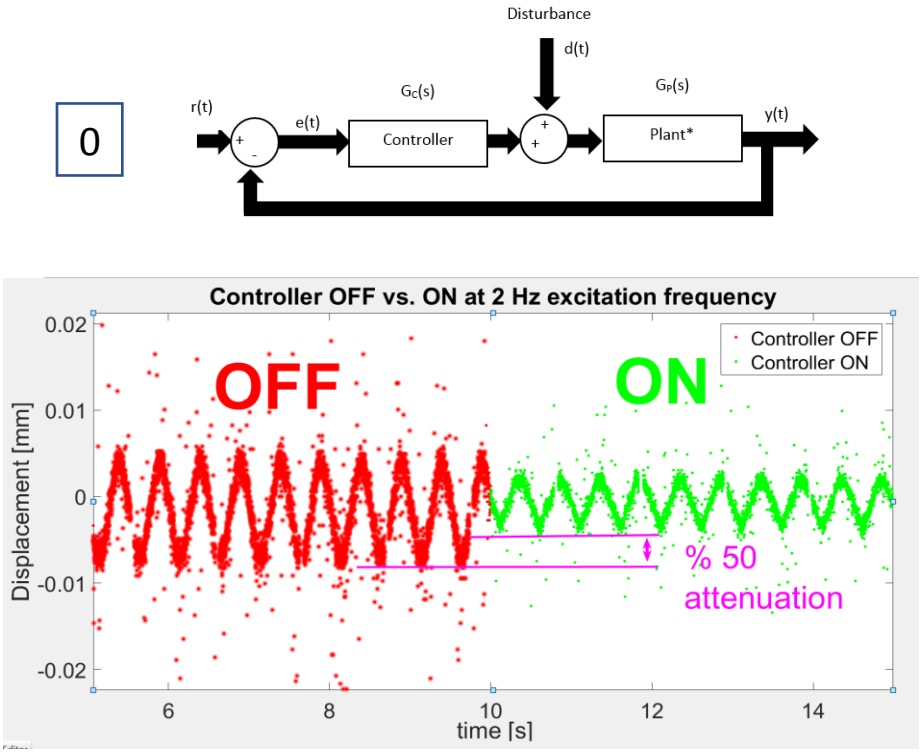

Figure 30 - In disturbance rejection, from r(t) to y(t) when the controller is ON and OFF at 2 Hz.

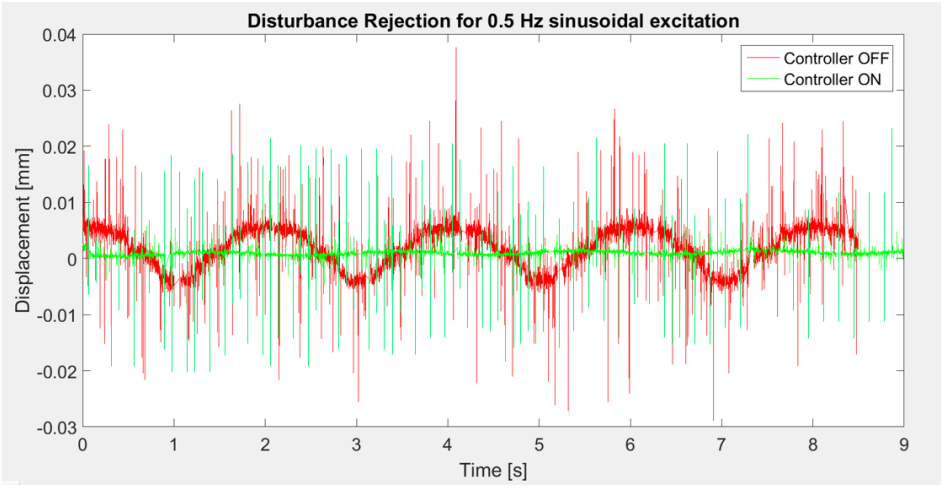

Figure 31 - In disturbance rejection, from r(t) to e(t) when the controller is ON and OFF at .5 Hz.

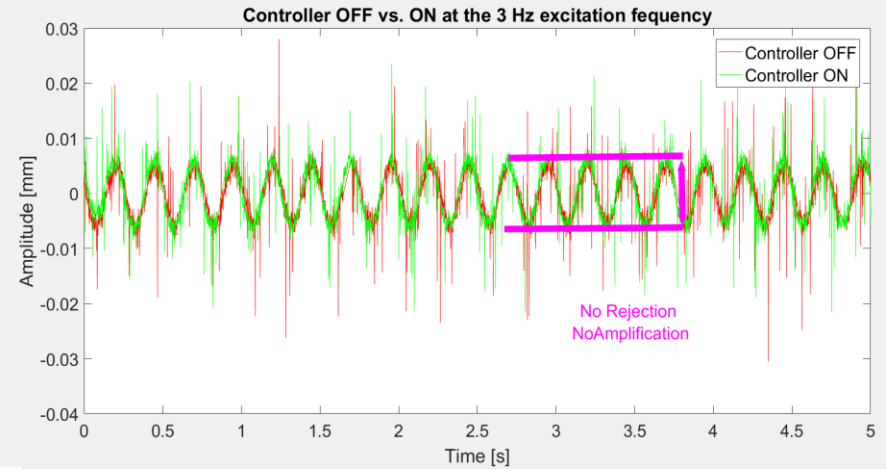

Figure 32 - In disturbance rejection, from r(t) to y(t) when the controller is ON and OFF at 3 Hz.

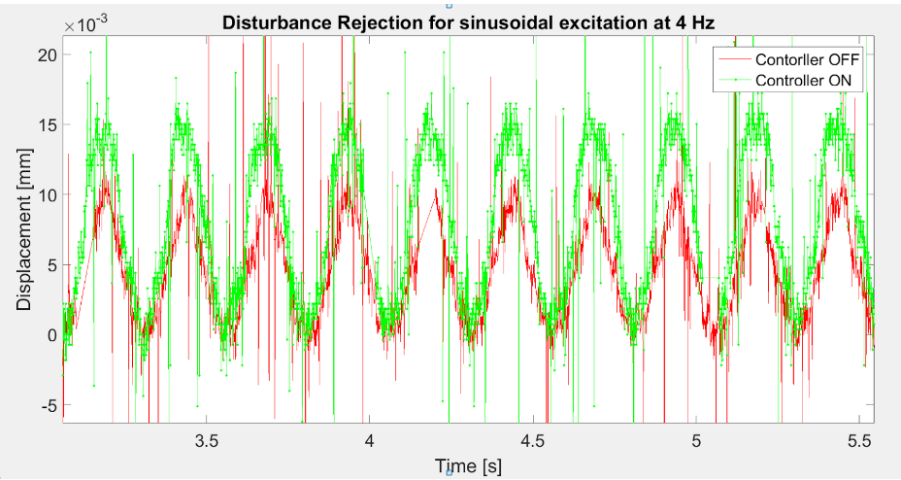

Figure 33 - In disturbance rejection, from r(t) to y(t) when the controller is ON and OFF at 4 Hz.

7.0 CONCLUSIONS

In this project, the data-driven control design method was used for active vibration control of a flexible mechanical structure. As the case study, a clamped-clamped beam configuration was used with multiple piezoelectric patch actuators bonded to it for creating disturbance excitations and controlling the vibrations. An experimental platform was developed with a set of piezoelectric actuators and sensors to validate the effectiveness of

the proposed method. A control optimization method was developed to obtain a disturbance-rejection closed-loop controller designed in the frequency domain. Experimental results indicate successful implementation of the developed controller for rejecting low-frequency disturbances.

8.0 FUTURE WORK

As the future extension of this project, the effect of hysteresis can also be integrated with the system to compensate for dissipating the energy in the piezoelectric actuator. Some improvement on the setup can be done, for example, the test bed can be designed to minimize the effect of gravity. More plants can be collected for a more robust control design. The controller can be optimized over more parameters to achieve a better performance level. The more advanced algorithm can be used to minimize the cost function. The cost function can be set with better weighing values. The discretization can be done in more sophisticated ways, for example, pole-zero-match rather than zero-order-hold. More accurate sensors or functional actuators can also improve the performance of the beam control system.

REFERENCES

[1] "Control engineering - Wikipedia," 2017.available: https://en.wikipedia.org/wiki/Control_engineering

[2] R. V. Dukkipati, *Analysis and design of control systems using MATLAB*: New Age International, 2006.

[3] S. BENNETT, "A history of control engineering 1800-1930 Control engineering series No. 8 UK, 1979. 227 p," ISBN 978-0-86341-047-5.

[4] C. Kilian, "Modern control technology. Thompson delmar learning," *Electron. Eng,* 2005.

[5] "Vibration control - Wikiversity," 2017. avalaible: https://en.wikiversity.org/wiki/Vibration_control

[6] S. Bashash, "Robust control optimization for high performance track following in hard disk drives," in *American Control Conference (ACC), 2015*, 2015, pp. 4634-4639.

[7] C. R. Fuller, "Experiments on reduction of aircraft interior noise using active control of fuselage vibration," *The Journal of the Acoustical Society of America,* vol. 78, pp. S88-S88, 1985.

[8] N. Kodera, H. Yamashita, and T. Ando, "Active damping of the scanner for high-speed atomic force microscopy," *Review of Scientific Instruments,* vol. 76, p. 053708, 2005.

[9] H. Gao, W. Sun, and P. Shi, "Robust Sampled-Data $ H_ {\ infty} $ Control for Vehicle Active Suspension Systems," *IEEE Transactions on Control Systems Technology,* vol. 18, pp. 238-245, 2010.

[10] S. Khot, N. P. Yelve, R. Tomar, S. Desai, and S. Vittal, "Active vibration control of cantilever beam by using PID based output feedback controller," *Journal of Vibration and Control,* vol. 18, pp. 366-372, 2012.

[11] T. Zhang, H. G. Li, G. P. Cai, and F. C. Li, "Experimental verifications of vibration suppression for a smart cantilever beam with a modified velocity feedback controller," *Shock and Vibration,* vol. 2014, 2014.

[12] M. S. Saad, H. Jamaluddin, and I. Z. M. Darus, "Active vibration control of a flexible beam using system identification and controller tuning by evolutionary algorithm," *Journal of Vibration and Control,* vol. 21, pp. 2027-2042, 2015.

[13] R. Weldegiorgis, P. Krishna, and K. Gangadharan, "Vibration control of smart cantilever beam using strain rate feedback," *Procedia Materials Science,* vol. 5, pp. 113-122, 2014.

[14] M. Mahmoodabadi, M. Taherkhorsandi, M. Talebipour, and K. Castillo-Villar, "Adaptive robust PID control subject to supervisory decoupled sliding mode control based upon genetic algorithm optimization," *Transactions of the Institute of Measurement and Control,* vol. 37, pp. 505-514, 2015.

[15] K. Zhang, G. Scorletti, M. Ichchou, and F. Mieyeville, "Phase and gain control policies for robust active vibration control of flexible structures," *Smart Materials and Structures,* vol. 22, p. 075025, 2013.

[16] K. Zhang, G. Scorletti, M. N. Ichchou, and F. Mieyeville, "Robust active vibration control of piezoelectric flexible structures using deterministic and probabilistic analysis," *Journal of Intelligent Material Systems and Structures,*

vol. 25, pp. 665-679, 2014.
[17] Z.-c. Qiu, "Experiments on vibration suppression for a piezoelectric flexible cantilever plate using nonlinear controllers," *Journal of Vibration and Control,* vol. 21, pp. 300-319, 2015.
[18] M. Gevers, "Identification for control: From the early achievements to the revival of experiment design," *European journal of control,* vol. 11, pp. 335-352, 2005.
[19] A. Bunse-Gerstner, D. Kubalińska, G. Vossen, and D. Wilczek, "h2-norm optimal model reduction for large scale discrete dynamical MIMO systems," *Journal of computational and applied mathematics,* vol. 233, pp. 1202-1216, 2010.
[20] S. Formentin, K. Heusden, and A. Karimi, "A comparison of model-based and data-driven controller tuning," *International Journal of Adaptive Control and Signal Processing,* vol. 28, pp. 882-897, 2014.
[21] S. Formentin, A. Bisoffi, and T. Oomen, "Asymptotically exact direct data-driven multivariable controller tuning," *IFAC-PapersOnLine,* vol. 48, pp. 1349-1354, 2015.
[22] H. Hjalmarsson, "Efficient tuning of linear multivariable controllers using iterative feedback tuning," *International journal of adaptive control and signal processing,* vol. 13, pp. 553-572, 1999.
[23] S. Formentin, S. Savaresi, and L. Del Re, "Non-iterative direct data-driven controller tuning for multivariable systems: theory and application," *IET control theory & applications,* vol. 6, pp. 1250-1257, 2012.
[24] A. Karimi and Y. Zhu, "Robust H∞ Controller Design Using Frequency-Domain Data," *IFAC Proceedings Volumes,* vol. 47, pp. 4921-4926, 2014.
[25] X. C. Méndez Cubillos and L. C. G. de Souza, "Using of H-infinity control method in attitude control system of rigid-flexible satellite," *Mathematical Problems in Engineering,* vol. 2009, 2010.
[26] S. Bashash, K. Vora, and N. Jalili, "Distributed-parameters modeling and control of rod-type solid-state actuators," *Journal of Vibration and Control,* vol. 17, pp. 813-825, 2011.
[27] M. Dadfarnia, N. Jalili, Z. Liu, and D. M. Dawson, "An observer-based piezoelectric control of flexible Cartesian robot arms: theory and experiment," *Control Engineering Practice,* vol. 12, pp. 1041-1053, 2004.
[28] E. Omidi and S. N. Mahmoodi, "Active vibration control of structures using a leader–follower-based consensus design," *Journal of Vibration and Control,* p. 1077546316631896, 2016.
[29] E. Omidi and S. N. Mahmoodi, "Active sensing of distributed parameter structures enhanced by robust consensus observer," in *ASME 2015 Dynamic Systems and Control Conference,* 2015, pp. V003T45A003-V003T45A003.
[30] G. F. Franklin, J. D. Powell, and M. L. Workman, *Digital control of dynamic systems* vol. 3: Addison-wesley Menlo Park, 1998.
[31] (2017). *Digital control - Wikipedia*. Available: https://en.wikipedia.org/wiki/Digital_control
[32] "White noise - Wikipedia," 2017.

APPENDIX

Characterizing the plant using FFT

The Fourier-Transform is one of the convenient and most straight-forward methods to characterize a signal. FFT is a numerical method which rapidly calculates the related Discrete-Fourier-Transform Matrices the Fast Fourier Transforms is previously defined in MATLAB as the $fft(signal)$. The fft is being used to transfer the output signal and input signal into the frequency domain. The benefit of using this method is an overall behavior of the system.

$$F(\omega) = \int_{-\infty}^{\infty} f(t) e^{-2\pi i \omega t}\, dt$$

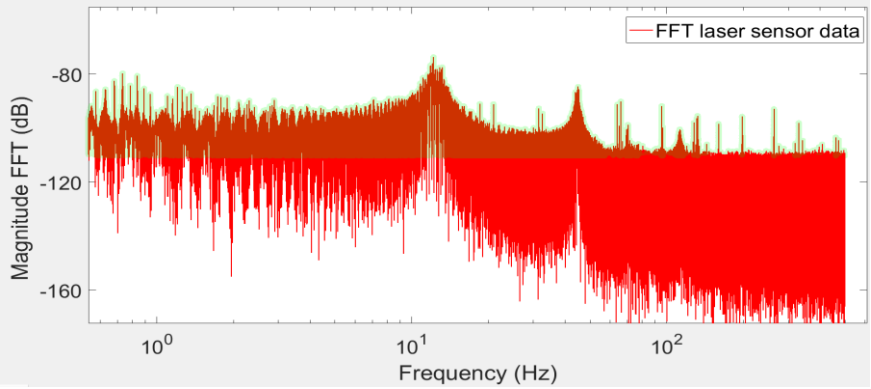

Figure 34 - The FFT response data of the output of displacement over the input of voltage.

The plant below is obtained by the division of the FFT of the output signal which is the laser sensor over the FFT of the input data which is voltage. The FFT length is from the entire of the spectrum up to the sampling frequency. for example, if the sampling time T_s be 0.001, then the sampling frequency is 1000 Hz. Getting FFT would provide the spectrum from 0 to 1000 Hz. Then, the second half of the data is the mirror of the first half. The data below is provided only for the first half of the data, for both input and output. In the formula for the transfer function of G, y and u are time dependent variables.

$$G(\omega) = \frac{fft(y)}{fft(u)}$$

The bulk red data which is scattered in the entire of the spectrum is due to the white noise. White noise is referred to a signal which has a persistent power spectrum density. In a discrete signal, is considered as of serially uncorrelated random variables with zero mean and limited variance [32]. To eliminate this effect the project would focus on the first proposed method.

Modal Analysis using Ansys

There are different approaches to find the response data. First is computational FEA modeling of the structure where the flexible beam is modeled with all details such as the actuators, end-clamps. Then, using modal analysis, the natural frequencies can be obtained. By harmonic response Ansys feature, the frequency response data can be obtained.

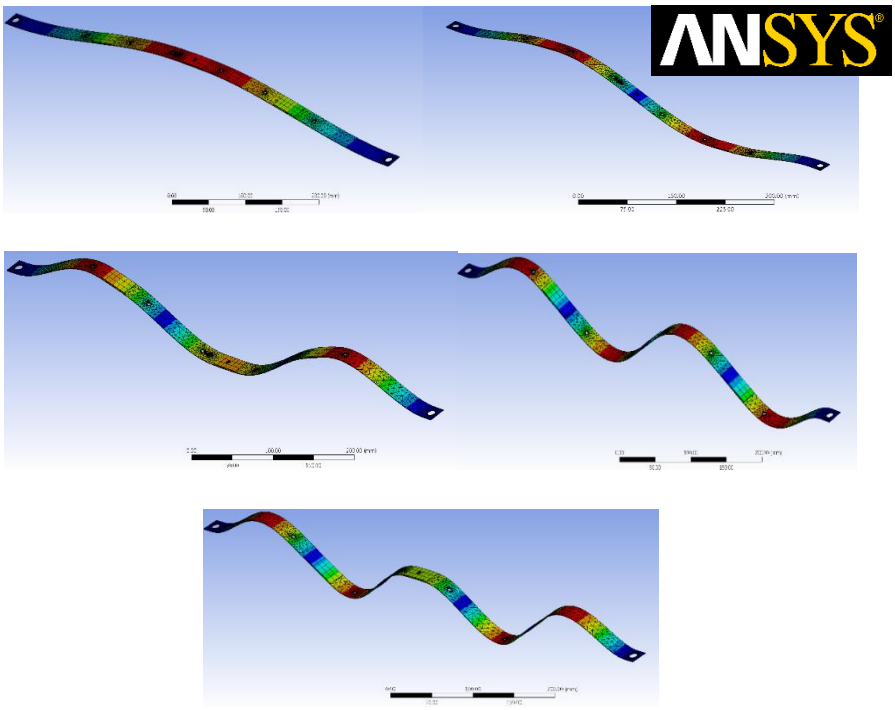

Figure 35 - The five first mode of a cantilever beam resulted from Modal analysis.

Table 4 - The comparison of resonant frequencies from the experiment and Ansys FEA.

The experimental results	The Ansys results
14 Hz	14 Hz
44 Hz	39 Hz
113 Hz	80 Hz